THE EXTRAGALACTIC DISTANCE SCALE KEY PROJECT I. THE DISCOVERY OF CEPHEIDS AND A NEW DISTANCE TO M81 USING THE *HUBBLE SPACE TELESCOPE*

W. L. FREEDMAN, S. M. HUGHES, B. F. MADORE
J. R. MOULD, M. G. LEE, P. B. STETSON, R. C. KENNICUTT
A. TURNER, L. FERRARESE, H. FORD, J. A. GRAHAM, R. HILL
J. G. HOESSEL, J. HUCHRA, G. D. ILLINGWORTH,

Submitted to the *Astrophysical Journal* June 23, 1993

ROBERT HILL
Carnegie Observatories
813 Santa Barbara St
Pasadena, California 91101
I: bhill@ociw.edu

JOHN G. HOESSEL
Department of Astronomy
University of Wisconsin
475 N. Charter St.
Madison, WI 53706
hoessel@uwfpc.span

JOHN HUCHRA
Harvard College
Center for Astrophysics
60 Garden Street
Cambridge, MA 02138
huchra@cfa3.span

GARTH D. ILLINGWORTH
Lick Observatory
University of California
Santa Cruz, CA **95064**
1: gdi@helios.ucsc.edu

[1]Based on observations with the NASA/ESA *Hubble Space Telescope,* obtained at the Space Telescope Science Institute, which is operated by AURA, Inc. under NASA Contract No. NAS 5-26555.

[2]Visiting Astronomer at the Canada-France-Hawaii Telescope, which is operated by NRC Canada, CNRS France, and the University of Hawaii.

[3]This paper is based in part on observations which were made at Palomar Observatory which is owned and operated by the California institute of Technology.

Received.....

A ddress for Proofs:
Wend y L. Freedman
The Observatories of the Carnegie institution of Washington
813 Santa Barbara St.
Pasadena, California 91101

Running Headline: *Cepheids in M81*

THE EXTRAGALACTIC DISTANCE SCALE KEY PROJECT. I. THE DISCOVERY OF CEPHEIDS AND A NEW DISTANCE TO M81 USING THE *HUBBLE SPACE TELESCOPE*[1]

WENDY L. FREEDMAN[2]
Carnegie Observatories
813 Santa Barbara St
Pasadena, California 91101
I: wendy@ociw.edu

SHAUN M. HUGHES[3], **BARRY F. MADORE**[2], **and JEREMY. R. MOULD**[3]
California Institute of Technology
Pasadena, California 91125
I: smh@pharlap.caltech.edu, barry@ipac.caltech.edu, jrm@deimos.caltech.edu

MYUNG **GYOON LEE**[3]
Carnegie Observatories
813 Santa Barbara St
Pasadena, California 91101
I: mglee@ociw.edu

PETER B. STETSON
Dominion Astrophysical Observatory
5071 W.Saanich Rd.
Victoria BC V8X 4M6
I: stetson@dao.nrc.ca

ROBERT C. KENNICUTT and ANNE TURNER
Steward Observatory
University of Arizona
Tucson, AZ 85721
I: robk@as.arizona.edu, aturner@as.arizona.edu

LAURA FERRARESE and HOLLAND FORD
Space Telescope Science Institute
Homewood Campus
Baltimore, MD 21218
I: ferrarese@scivax.stsci.edu, ford@scivax.stsci.edu

JOHN A. GRAHAM
Department of Terrestrial Magnetism
Carnegie Institution of Washington
5241 Broad Branch Rd. N.W.
Washington D.C. 20015
I: graham@dtm.dnet.nasa.gov

ABSTRACT

We report on the discovery of 30 new Cepheids in the nearby galaxy M81 based on observations using the Hubble Space Telescope (HST). The periods for these Cepheids lie in the range of 10 to 55 days, based on 18 independent epochs using the HST wide-band F555W filter. The HST F555W and F785LP data have been transformed to the Cousins standard *V* and *I* magnitude system using a ground-based calibration. Apparent period-luminosity relations at *V* and *I* were constructed, from which apparent distance moduli were measured with respect to assumed values of μ_0 = 18.50 mag and *E(B- V)* = 0.17 mag for the Large Magellanic Cloud. The difference in the apparent *V* and *I* moduli yields a measure of the difference in the total mean extinction between the M81 and the LMC Cepheid samples. Our data indicate a total mean extinction to the M81 sample of *E(B- V)* = *0.11* msg. The true distance modulus to M81 is determined to be 27.80 ± 0.20 mag, corresponding to a distance of 3.63 ± 0.34 Mpc.

These data illustrate that with an optimal (power-law) sampling strategy, the HST provides a powerful tool for the discovery of extragalactic Cepheids and their application to the distance scale. M81 is the first calibrating galaxy in the target sample of the HST Key Project on the Extragalactic Distance Scale, the ultimate aim of which is to provide a value of the Hubble Constant to 10% accuracy.

Subject headings: galaxies: individual (M81) - galaxies: distances - stars: Cepheids

1. INTRODUCTION

A convincing determination of the Hubble Constant (il.) remains today as one of the major unsolved problems in observational cosmology. Because of its importance, the determination of H_0 was designated as one of the Key Projects for the *Hubble Space Telescope* (11ST). While debate over HO continues, as it has for the last half century, it is perhaps more sharply focused than ever before (e.g., Fukugita, Hogan and Peebles 1993): distances to galaxies within the Local Group (1 Mpc) are no longer in dispute, but substantial disagreement occurs as distances approaching that of the Virgo cluster ($\sim$ 15 Mpc) are reached.

The goal of the Extragalactic Distance Scale Key Project is to address this observational discrepancy. The Key Project is designed to obtain accurate and uniformly-determined distances to nearby galaxies using Cepheid variables, and thereby to provide a secure database which will be accessible to the entire astronomical community for the calibration of the extragalactic distance scale. Most of the observations of the distant target galaxies of the Key Project have been delayed due to the spherical aberration of the HST primary mirror. However, despite this problem, HST has turned out to be efficient at the detection and discovery of Cepheid variables in the nearer galaxies in the sample. Here we report our first observations inducting the discovery of 30 Cepheids (and the recovery of one known Cepheid) in the nearby galaxy M8 , made using the Wide Field Camera (hereafter referred to as WFC).

M81 was chosen as a target galaxy because of its proximity based on the high degree of resolution of its spiral arms and ground-based distance estimates - see §6), and for its potential in providing a calibrator simultaneously for several secondary distance indicators. Located at α_{1950} = 09}' 51^m, δ_{1950} = +69° 18', (l = 142°, and b = 410), M81 is classified as Sb(r)I-II by Sandage and Tammann (1981), and is similar in many respects to the Local Group galaxy M31. The high inclination of its disk (58°) and its well-defined 21-cm velocity width make M81 an

important Tully-Fisher calibrator, while its relatively large bulge makes it useful as a calibrator of surface-brightness fluctuations and the planetary nebula luminosity function. Very recently a type 11 supernova (SN 1993J) was discovered in M81, offering a potential cross-check for, and empirical calibration of, the expanding photosphere method. Also, it has been suggested that the bulge luminosity of M81 can be used to calibrate the D_n–Σ relation for SO and elliptical galaxies (Dressier 1987).

2. THE CEPHEID OBSERVATIONS

2.1 Search Strategy

Prior to this HST survey, two Cepheids were known in M81 (Sandage, private communication). Thus it is obvious that the brightest Cepheids in M81 can be observed from the ground; however, in practice this task has proven to be very difficult. The high-surface-brightness background and extreme crowding of stellar images in the arms of M81 have posed severe problems for the ground-based identification of variables.

A space-based search for variable stars has several distinct advantages over ground-based studies. Even with spherical aberration of the HST mirror, the sharp cores of the stellar images can be used successfully to measure accurate magnitudes and discover variables. Much of this success is also due to the stability of the point-spread function over time (as compared to terrestrial seeing variations), and to the ability of 11S'1' to successfully re-acquire field centers and orientations to within a fraction of a pixel. However, one of the greatest advantages of 11ST over ground-based efforts (beyond its eventual superior resolution) is its ability to be scheduled optimally and independently of considerations such as phase of the moon, time of day, weather and seeing variations. This optimal scheduling significantly reduces the number of observations needed to identify variables and to determine their periods unambiguously. Moreover, it simultaneously

allows uniform coverage of the light curves so that well-determined amplitudes, mean magnitudes, and colors can be extracted.

Details of the HST Key Project sampling strategy will be described in a forthcoming paper (Madore and Freedman 1994), but the following summarizes the method applied to the specific case of M81. Simply stated, the general sampling problem is this: Given an unknown population of variable stars whose periods can lie continuously anywhere in a specified range (P_{min} to P_{max}), what is the optimal spacing in time of a fixed number of observations N, when these observations are constrained to lie within a finite and fixed window of duration T? 'Optimal spacing' in this context simply means that the number of redundant phase points is minimized. For example, sampling a particular light curve only at maximum might be useful for determining a period, but it would yield significant and systematic errors in the mean magnitude. (Furthermore, such data would be useless for discovering any Cepheid with that period or any period which was shorter by an integral factor.) Phase spacing as close to uniform as possible was sought for all variables over the specified range of periods from P_{min} = 10 to P_{max} = 100 days, within the imposed M81 observing window of T = 45 days. Ultimately we adopted a power-law distribution of sampling within the initial 45-day observing window. Extensive simulations were run to determine the optimal power-law exponent given the constraints of time interval, number of observations, and period range expected. Initial simulations for the originally expected signal-to-noise ratios for the WFC indicated that a sequence of 12 V-band observations within the observing window, followed up by a return visit one year later, would provide periods accurate to 10%. When the larger photometric errors due to the spherical aberration became known, further simulations were run that indicated that additional observations should be obtained in Cycle 2. A sequence with a total of 18 *V*-band observations was finally adopted.

Figure la shows a plot of the optimization diagram resulting from the specific observing pattern adopted for the first cycle of Cepheid observations in M81. The range of potential Cepheid periods are plotted along the x-axis. The y-axis is a measure of the variance of the phased data. The variance plotted is a normalized measure "of the degree to which the observed phase sampling deviates from that of ideal phase sampling, where the ideal observations fall uniformly around the light curve, without any redundancies. The sum of the squares of the differences between phase-ordered adjacent pairs of data points are calculated and then normalized to the same quantity calculated for the ideal phase sampling. The normalization is such that zero variance corresponds to the case where the data, after phasing to a given period, result in a light curve that is sampled at equally spaced phase points containing no redundancies. For comparison, the results of a uniformly spaced sampling rate consisting of the same number of data points in the same time interval is shown in Figure lb. Extreme downward deviations indicate data clumping (and a loss of information through redundancies) clue to resonance between the sampling frequency and those particular Cepheid periods. Comparison with Figure la shows that the sampling strategy adopted here eliminates these major deviations. Moreover, within the period range of interest, the variance, in the mean, is independent of period. Figures 2a and 2b show the best and the worst sampling of a Cepheid light curve predicted for this set of parameters. Figure 2 is a graphic illustration of the power of scheduling in general, and of the efficiency of HST in specific, for the discovery of Cepheids and their application to the extragalactic distance scale. Considerably more effort would be required from the ground to achieve comparable sampling.

In addition to the issue of sampling, another important. element in the search for Cepheids is the choice of bandpasses for the observations. Several factors must be taken into consideration, including the known, intrinsic properties of Cepheids, the sensitivity of available detectors, and the total amount of observing time required. The amplitudes of Cepheids decrease with increasing

wavelength (e.g., Wisnewski and Johnson 1968; Freedman, Grieve and Madore 1985); hence, Cepheids arc best discovered at short wavelengths where their amplitudes are largest. However, at these shorter wavelengths, proportionately more observations are required to obtain accurate mean magnitudes, compared to longer wavelengths where the amplitudes are smaller and the individual magnitudes are statistically closer to the mean. And perhaps most importantly, as emphasized over a decade ago, the complicating effects of extinction are decreased as longer wavelengths are chosen (McGonegal *et* al. 1982).

The HST bandpasses chosen were F555W (approximately Johnson *V*) and F785LP (approximately Kron-Cousins *I*). At the short wavelength end, the V-band filter was chosen as the bandpass to carry out the variable search as a compromise between the competing effects of amplitude, reddening, and chip sensitivity. The. amplitudes of Cepheids are known to be 30% larger at *B* than at *V*; however, the sensitivity of the WFC chips drops precipitously at *B*, and reddening is a factor of 1.3 larger at *B* than at *V*. Thus there is a clear advantage to *V* over shorter wavelengths in terms of chip sensitivity and lower reddening, but it is less satisfactory when consideration is given to the amplitudes. Nevertheless, Cepheid amplitudes are generally still large at *V* and are a factor of 2 larger than at *I* so that the detection probability is not severely compromised. Eighteen V-band observations were obtained for the variability y search, and six additional *I*-band observations were also acquired. Fewer *I*-band observations are necessary because of the factor of 2 decrease in amplitude; hence the error on the mean (due to intrinsic variability) is similarly reduced. Moreover, once a period and an amplitude are determined from the *V* data, the *I*-band data can then be phased and scaled so that even with fewer observations, a mean *I* magnitude can be determined with a precision comparable to the mean *V* magnitude (see Freedman 1988; Freedman, Wilson and Madore 1991).

2.2 Observations

The HST observations of two fields in M81 were begun with the WFC on 30 December 1991. The wide-band filter F555W (V) and the long-pass filter F785LP (*I*) were used to obtain twelve and four epochs, respectively, within the initial 45-day interval. A second observing sequence was begun on 28 December 1992, adding 6 more F555W and 2 additional F785LP exposures.

The WFC consists of four separate 800x800 CCD detectors, and each pixel (15μm) subtends O'! 10 on the sky, so that the total field of view of the camera is 2! 6 x 2! 6. Detailed descriptions of the WFC can be found in the HST/WFPC Instrument Handbook, Version 3.0 (MacKenty *et al.* 1992). All observations were obtained with the telescope guiding in coarse track, which has a performance in the range O'! 025 and O'! 130, depending on the brightness of the guide stars.

The area covered by the two 11ST WFC fields is illustrated in Figure 3, superimposed on a B-band print of a photographic plate of M81 obtained at the CFHT in February, 1983. The first field was chosen to be located along the major axis at the northern end of the galaxy; the second field was chosen to contain the known Cepheid V30 and is located to the east approximately along the minor axis.

Exposure times for the F555W frames were generally 1200 see, with the exception of 4 images which were split in two with the intent of facilitating cosmic ray removal. The exposure times for the cosmic-ray split frames were 900 sec each. Exposure times for the six F785LP observations for each field were 1800 sec each. In Figures 4a-d and 5a-d, images of the median of the 22 F555W exposures for each chip in both fields are displayed. The individual images were photometrically scaled and geometrically transformed to a common zero point for this purpose. Only those regions of the image which appear in at least 10 of the 22 images are included.

3. DATA REDUCTION

3.1 Pre-processing

Routine calibration of the data was carried out by the science data-processing pipeline system maintained by the Space Telescope Science Institute. The calibration process is described by Lauer (1989). Four calibration steps were performed in the following order: statistical correction for problems introduced in the analog-to-digital conversion, bias subtraction, dark subtraction, and flat field division. The analog-to-digital correction removes the systematic degradation introduced by the analog-to-digital conversion electronics. The structure built into the electronic bias is removed by subtracting a bias frame obtained in orbit from the average of a set of individual bias readouts. The dark frame is constructed from orbit-long dark exposures; the nominal value for the CCD dark current is 0.003 electrons/pixel/second. Finally, the division by the flat field frame corrects for variations in sensitivity between pixels in the CCD detector. Flat fields were obtained for the different filters by observing the bright Earth surface as it passes below the spacecraft.

The flat fields used here were last updated by STScI in early 1992, after the first images in the program had been taken. To ensure a consistent calibration for all of the data, all the images taken before the flat-field update were recalibrated using the same stepping procedures described above using the newest set of calibration files. As described in §3.3 and §5.2, we later tested for systematic effects in the zero-point calibration and the period-luminosity relations using flat-field frames obtained as part of the Medium Deep Survey by Phillips (Lick MDS Report No. 3). Finally, spurious effects related to internal scattered light due to contaminants (a problem known as measles) have been searched for in our images, but were not detected.

3.2 Instrumental Magnitudes

Data reduction for this project was performed with DAOPHOT (Stetson 1987) and the related software packages ALLSTAR and ALLFRAME. ALLFRAME is a recent extension of the DAOPHOT/ALLSTAR method of obtaining photometry from digital images using model-profile fitting. It was developed in an attempt to make the best possible use of the information in multiple digital images for projects involving faint stars and/or crowded fields, including the Cepheid target fields of the Extragalactic Distance Scale Key Project; details of the program will be described by Stetson (1993, in preparation). Here we provide a brief summary of the method used to obtain the M81 photometry.

Like NSTAR and ALLSTAR, ALLFRAME derives estimates of stellar magnitudes using a robust least-squares-like fit of a model point-spread function (P SF) to actual observed' brightness values within a star's profile in' a digital image. While NSTAR fits multiple profiles simultaneously to small groups of mutually overlapping star images, ALLSTAR performs NSTAR-like simultaneous profile fits for all stars in an entire digital image. ALLFRAME extends this progression by performing multiple, simultaneous profile fits to all star images in a full ensemble of CCD frames of a given field. For a given field of sky, ALLFRAME accepts a list of CCD images and provisional geometric transformation equations interrelating the coordinate frames of those images. ALLFRAME also accepts as input a *single* star list for that field. The reductions then proceed as AI, LFRAME performs profile fits to obtain the apparent magnitude (and the underlying diffuse sky brightness) for each star in each image, while requiring that each star have a consistent position in all of the images in which it appears. At the same time, ALLFRAME makes modest corrections to the provisional frame-to-frame geometric transformation constants, including quadratic terms in x and y if desired.

No particular precautions were taken to deal with the cosmic rays in our images. ALLFRAME,

like all of the DAOPHOT profile-fitting packages, uses an automatic down-weighting of discrepant data points (see Stetson 1987). Moreover, this method of making the photometry more robust against corrupt data is far more effective with ALLFRAME than with PEAK, NSTAR, or ALLSTAR, since the requirement for frame-to-frame consistency in a given star's centroid position results in far more independent pixels per degree of freedom in the fits. A cosmic ray or other defective pixel in the wing of a star image thus has less influence on the fit to begin with; it stands out more obviously as defective and as a result is more reliably down-weighted, thus rendering it still less significant in the end. Only in the case of a cosmic ray hit squarely on the centroid of a star image will it be difficult or impossible to distinguish between defective data and a true temporary brightening of the star. However in these cases, a light curve can ultimately discriminate between such spurious events and a true Cepheid candidate.

The M81 HST images present many new challenges for DAOPI1OT reduction. For WFC images, the profile fits are dominated by the core of the image, which is much less than two pixels in radius and contains on the order of 15% of the flux. However, this core is surrounded by a halo of flux which, although it has a low surface brightness, extends measurably out to a radius of ≈ 25 pixels. This halo covers so much area ($x(25)^2 \approx 2000$ square pixels), that an error of a few tenths of an ADU in the mean sky brightness can produce an error in the total volume of the PSF which is a large fraction of the flux in the profile core. Although this presents a problem for absolute stellar photometry, DAOPHOT handles this difficulty by restricting PSF fitting for relative photometry to a radius of 2 pixels. Furthermore, with comparatively few bright stars in the M81 fields, a low dynamic range, an adverse core/halo structure in the PSF, and dust lanes and other actual underlying sky-brightness variations on spatial scales of the same order as the radius of the PSF, it is extremely difficult to obtain a point-spread function acceptably free of variations in the core/halo ratio. Thus from the outset, it was clear that a great deal of experimentation would be required to

arrive at the best possible way of defining the PSFs for these analyses. Accordingly, the task was divided so that the 'Major Axis Field' images were reduced with an empirical PSF derived from the science frames themselves, while the 'V30 Field' images were reduced with PSFS derived from numerical "tinytim" simulations (Version 2.1 kindly provided by J. Krist, Space Telescope Science Institute) of the telescope optics.

The empirical PSI? for the major-axis reductions was obtained as follows. All available major-axis V-band (F555W) images from WFC chips 1 and 2 were medianed together (after suitable transformations for translation, rotation, and differences in their exposure times and instantaneous sensitivity). Then these two images were added together to create a combined image with twice the surface density of stars bright enough for the estimation of the average frame's PSI?. The standard DAOPHOT technique of determining a provisional PSF from bright stars, using that PSF to subtract the faint stars around and within the profiles of the bright stars, and then determining a new PSF from the '(cleaned" images of the bright stars, was used to derive an average PSF that allowed for quadratic spatial variations in the profile (Stetson 1991a, b). The same procedure was followed using the medians of all available I-band (F785LP) major-axis images from WFC Chips 1and 2. These two PSFS were then employed in ALLFRAME reductions of all the major-axis images from the four chips.

The theoretical I'SF for the 'V30 Field' reductions was obtained by using the "tinytim" code to generate a grid of synthetic star images in a blank frame. The l) AOPHOT "PSF" routine was then used to generate a numerical point- spread function suitable for use with the DA OPHOT software, just as if this had been a real image obtained in the normal way. A separate PSF was generated for each of the two filters and each of tile four chips. l'experiments were also performed to see whether it would be advantageous to generate a separate PSF for each observing epoch, taking into account known variations in the telescope focus. It was found that these focus variations produce changes

in the derived magnitudes that are small compared to other irreducible sources of noise, such as the readout noise of the chip. Therefore, to save effort, one approximately average PSF was used for all epochs with each chip/filter combination. These eight PSFS were then employed in AI, LFRAME reductions of all the 'V30 Field' images.

We are continuing to work on improved characterization of the WFC PSF. Alternative representations can be evaluated from the residuals from our fit to the secondary standards or indeed any WFC images of high S/N with suitably different telescope pointings. We find that within 300 pixels of chip centers different PSFS yield magnitudes with *rrns* differences of 0.06 msg. 'l'his covers just over half the effective field. Over the field as a whole we see *rms* differences up to 0.15 msg. Improved PSFS should lead to a reduction in these field effects, but are not expected, given the large number of secondary standards we are employing, to change the zeropoint of our photometric calibration (§3.3) significantly.

3.3 Calibration

The main problems affecting calibration of WFC magnitudes are (1) errors in the flat fields, (2) inadequate modeling of the variation of the PSF across the field, and (3) the time variation of detector sensitivity due to contamination. The problems are thoroughly discussed in the WF/PC Final Orbital/Science Verification Report (Faber and Westphal *et al.* 1991, the 'IDT Report'). To deal wit h these problems we have chosen to calibrate our fields from the ground. A ground; based calibration has the virtue of protecting our results from systematic error due to any of these causes, although our random errors will still depend on how well these three effects are understood. Calibration data were acquired at a number of facilities including the Canada- France- Hawaii telescope (CFHT), the Palomar 5m (1'200) and the Palomar 1.5111 (1'60) telescopes.

The zero-point calibration of the WFC data. is complicated by several factors. Due to the fact

that all four cameras of the WFC are re-imaged separately onto independent chips, the relative zero points of the four output frames are different. Thus each of the four CCD images needs to be calibrated individually. The accuracy with which these calibrations can be carried out depends on the degree of overlap with the ground-based CCD frames, and on the numbers of available bright but unsaturated, isolated stars common to the two data sets, with which to tie in the photometry.

BVRI observations of the fields containing the two known M81 Cepheids, V30 and V2, were acquired at the CFHT on 19/20/21 January 1988. The l-band data for these Cepheids were published by Freedman and Madore (1988); the *BVRI* data for these fields have more recently been presented by Madore, Freedman, and Lee (1993). The photometric tie-in to the 11ST data was carried out using only stars which appear as single, isolated images on both the CFHT and HST frames. The 2! 3 x 3! 5 area covered by the CFHT V30 CCD frames overlap with all four of the WFC chips for the HST 'V30 Field'. The coverage of Chips 1 and 4 is excellent; however, the coverage of Chips 2 and 3 is limited.

Supporting data were obtained at the P60 by MGL on 26 June 1992. For 3 bright, isolated stars in common to the CFHT and 1'60 frames, these data confirmed that the CFHT calibration was secure at a level of 0.03 mag at Vand 0.01 mag at *I*. Further confirmation that the CFHT night was photometric and the calibration reliable was available from data independently obtained at the Kitt Peak National Observatory (KI'NO) 4m for NGC 2403 on 23 March 1984. Frames of NGC 2403 were also acquired at the CFHT on the same photometric night as the M81 data (Freedman and Madore 1988; Madore, Freedman and Lee 1993). The independent KPNO and CFHT data for NGC 2403 agree to better than ± 0.02 mag for *BVR* and *I*, again indicating that both nights were photometric and well-calibrated.

Finally, an independent determination of the zero point of the }1S'1' data was obtained using the 1'200 with the COSMIC CC]) camera (built recently by A. Dressler and B. Kens). Details of

this calibration will be presented in Hughes *et al. (1993).* On 8 and 9 June 1992, JRM obtained *V* and *I* data for both of the HST fields, in addition to observations of standard star fields (Landolt 1992; Christian *et al.* 1985), The nights appeared to be photometric but notes of thin haze were recorded in the log book. A comparison of the CFHT and COSMIC photometry for the HST field containing V30 yielded agreement at levels of 0.05 ± 0.03 and 0.06 ± 0.03 mag in *V* and *(V-I)* respectively.

From the sources described above we have a total of 74 secondary standard stars with *V* and *I* photometry in our M81 fields. First, we examined the differences between *V* and $F555W_{ALLFRAME}$ for these stars. We neglected the color difference between the V and F555W systems, which according to Harris *et al.* (1991) varies smoothly from zero to only 0.05 mag for stars with *(B-V)* in the range of 0.0 to 1.0 msg. Direct transformation from $F555W_{A1,1JFRAME}$ to *V* in this manner may involve slightly larger random errors, but will lead to no systematic errors provided the mean color of our secondary standards is similar to the mean color of the Cepheids. Hughes *et al.* (1993) show that this amounts to F555W -- V < 0.01 msg.

'l'able 1 indicates these differences ($V - F555W_{ALLFRAME}$) for each of the 4 chips. The fact that these differences are significant is due most likely to errors in the flat fields, and incorrect characterization of PSF variation. Our primary calibration technique, however, sidesteps these problems.

We have a check on these numbers from a second calibration technique based on the work of the IDT. We take into account the following effects: (1) In 'l'able 12.15 of the IDT Report the sensitivity of WFC at F555W on 30 December 1991 (the epoch to which our AI, I, FRAME magnitudes are normalized) was found to be 0.15 mag lower than the calibration baseline sensitivity. This is confirmed by Ritchie & MacKenty (1993). (2) The aperture correction from ALLFRAME magnitudes to total (25 pixel radius) magnitudes is measured to be 1.60 msg. (3) The baseline

sensitivities of the individual WFC chips is given in Table 12.13 of the IDT Report. Combining these quantities, the second column in 'I'able 1 contains these zero-point estimates, which are in agreement with those obtained from our ground-based calibration. The agreement is somewhat fortuitous considering the uncertainty in the aperture correction. We adopt the primary direct calibration without modification.

'J'he color term between Kron-Cousins *I* and F785LP is larger (0.2 mag between *(V-1)= 0.0* and 2.0), and we take account of it explicitly. We transformed the (V, *I*) values of the M81 secondary standards to F785LP using the equation given by Harris *et al. (1991).* The magnitude differences $F785LP - F785LP_{ALLFRAME}$ are given in Table 1. A satisfactory calibration has been achieved in F785LP for Chips 3 and 4, but the uncertainty is over a factor of 2 higher for Chips 1 and 2. Zero-point estimates based on the IDT report (and an aperture correction of 2.04 mag) do not agree well with these values. Again, we adopt the primary direct calibration without modification.

In the face of these uncertainties we have tried to improve our calibration in the following ways. First, we tested the effect on 11ST magnitudes of alternative flat-field frames constructed by Phillips (Lick MDS Report # 3) from *Medium Deep Survey* data. Although use of these flat fields modifies the magnitudes of individual stars by up to 0.15 mag, the individual chip zero points are changed by only 0.02 mag *rms*, which is not significant, and the mean zero point change is less than 0.01 msg. Second, we have looked for a systematic difference in zero point between the 'Major Axis Field' with its empirical PSF and the 'V30 Field' with the "tinytim" PSF. We find a difference of +0.07 ± 0.07 mag in *V*. In F785LP the scatter between chips is larger, with a mean difference of +0.10 ± 0.26 msg.

The current calibration is adequate for present purposes, but improvements can be expected from better characterization of field effects in these data.

The zero points given in Column 3 of Table 1 can be used to transform the instrumental

ALLFRAME magnitudes onto a calibrated F785LP photometric system. To obtain calibrated *I* photometry of the Cepheids, (§ 4.2 below) the following procedure was used. The mean *I* magnitudes were calculated from the mean F785LP magnitudes using the transformation equation in Harris *et al.* (1991):

$$I = \mathrm{F785LP} + 0.0549\ (V\text{-}I) + 0.0343\ (V\text{-}1)^2$$

The final *I* magnitudes were determined by an iterative procedure using the above equation and an initial estimate of *(V–I)* given by (*V*–F785LP). Convergence typically required 4 iterations, where convergence was defined to have occurred when the change in the estimate of the *I* magnitude was less than 0.001 mag between two iterations.

4. VARIABLE STARS

4.1 Criteria

Two independent methods were used to search for the variables in the HST frames. in the first method, candidates were flagged on the basis of their mean magnitudes having a high internal dispersion for that magnitude relative to other constant stars. In the second method, variable candidates were chosen on the basis of a statistic sensitive to correlated magnitude residuals following Welch and Stetson (1993). The overlap in the two candidate lists was excellent; the best candidates were flagged independently as high probability Cepheids in over 90% of cases. The Cepheids were selected from these candidates on the basis of their phased and plotted light curves. In practice, if the average of the absolute deviation from the mean for a given star exceeded 1.5 times the mean ALLFRAME error for the eighteen epochs of photometry for that star, and if more than one point contributed to the large absolute deviation (thereby screening out obviously spurious candidates), the data were searched for best-fitting periods, phased, and then the light

curves were visually inspected for that star. Finally, the variable star candidates were inspected on the original CCL) images to flag, and in some case, exclude, those images located close to very bright stars.

The periods for each of the variable stars were determined using the Lafler and Kinman (1965) method of phase dispersion minimization (see also Stellingwerf 1978). The algorithm was modified slightly to allow for the errors in the individual data points. In addition, the absolute deviation (rather than the variance) in magnitude between adjacent phase points for various trial periods was calculated. Since the amplitudes of the Cepheids at *V* can exceed one magnitude and typical light curves are quite asymmetric, large differences in magnitude between adjacent phase points are not necessarily incorrect; in fact, they are expected. For each candidate variable, the data were phased for all periods between 2 and 400 days in incremental steps of 0.1 days. Light curves were plotted not only for the value of the period with the minimum phase dispersion, but also for the nine smallest values of that statistic. Once an approximate period was determined, it was refined by redoing the period search in increments of 0.01 days. Although in most cases the final periods adopted had the minimum value of the dispersion in phase, in some cases an obvious improvement to the light curve was obtained for other values,

Despite the pre-determined sampling strategy, it was not possible to completely eliminate aliasing problems for some of the periods. The basic data set consisted of 16 observations over 42 days in Cycle 1 followed approximately 11 months later by 6 observations over a similar interval in Cycle 2. The Cycle 1 observations thus carried the most weight in defining the basic light curves while the Cycle 2 observations were useful for refining the periods and for reducing aliasing. For some stars, particularly those with short periods near 10 days, the 11 month interval was too long to uniquely determine the number of cycles between the two data sets. For a few other stars (e. g., Cepheid C6 in the 'Major Axis Field' Chip 2) pure chance distribution of phases conspired to

produce ambiguous periods. In almost all cases, we could express a preferred value but when a second possible period exists, we have noted it.

Several of us independently inspected the light curves using several potential periods in order to minimize problems due to aliasing. Furthermore, we were able to assess visually the effect of isolated bad data points on the light curves and period determinations. When we came to compare conclusions, we found close agreement and the few differences were easily resolved by discussion.

The newly-discovered Cepheids are identified for each of the fields in Figures 4 and 5. In addition, smaller-area finder charts for each of the individual Cepheids are displayed in Figure 6. These finder charts cover a region of 50 x 50 pixels, (5"X 5") and are oriented in the same way as each of the chips displayed in Figures 4a-d and 5a-d. Note that the greyscale mapping is independent for each subset image so that the relative magnitudes for the Cepheids cannot be deduced from an inspection of these images.

Periods for the Cepheids are listed in Column 4 of Tables 2 and 3 for the 'Major Axis' and 'V30' fields, respectively. Also tabulated are the Cepheid ID number, x and y positions on the individual WFC chips (measured in pixels from the lower left corners as labeled in Figures 4 and 5), intensity-mean V and I magnitudes, a phase correction to the I data (described in §4.2 below) and N_{sig} (the factor by which the average of the absolute deviation from the mean for that Cepheid exceeded the internal mean error of the photometry for the eighteen epochs of V data). In the Notes to Tables 2 and 3, comments on the presence of nearby companions, and second possible periods, where appropriate, are given. The periods for these M81 Cepheids range from 10 to 55 days. The previously known Cepheid V30 (= C27 in this paper) was recovered, and its period agrees very well with the 30-day period determined by Sandage (1986, private communication).

In Tables 2 and 3, not all of the Cepheids have I magnitude entries. In the Major Axis Field, 2 out of 24 Cepheids were not found by ALLFRAME at I (C16 and C24). In the case of C4,

the errors at *I* were too large for a reliable mean to be determined. An even larger fraction of Cepheids (30f the 7) in the V30 Field were not recovered at *I*. Unfortunately, for reasons that arc not well-understood, in the case of the V30 Field, there were large positional offsets (in one case amounting to $\sim$ 100 pixels) between the frames taken at different epochs. Subsequently, the ALLFRAME coordinate list for the V30 Field was generated from a median of the *I* images, with the end result that stars along the frame edges do not all have measured *I* magnitudes (including C25, C27 (= V30) and C31).

The *V* photometry for the individual Cepheids is given in Table 4 which lists the Julian date of each observation, the *V* magnitude, and the AI, I, FRAME error in the *V* magnitude. The corresponding *I* photometry follows in Table 5.

In addition to the Cepheids discovered (and recovered) in these fields, many other variables were also found. Most of these additional stars appear to be long-period variables with periods in excess of 100 days, and at present we do not have sufficient phase coverage to determine reliable periods for them. Follow-up observations of these long-period variables are underway. Finally, 2 probable and 1 definite, eclipsing variables were found.

4.2 Light Curves and Mean Magnitudes

Light curves for each of the Cepheid candidates located in the 'Major Axis Field' are plotted in Figures 7a-f for Chips 1 to 4, respectively. The corresponding plots for Cepheids in the 'V30 Field' are displayed in Figures 8a,b. Fewer candidates were found in the 'V30 Field', consistent with the fact that the surface density is lower over much of the field (see Figure 3). Variables in the plots are labeled with their ID numbers and periods. The light curve of the eclipsing variable is illustrated in Figure 9, and its position, mean magnitude and period arc presented in Table 6.

By design our sampling is very uniform with respect to phase, and therefore fitting light curves

to the data to determine mean magnitudes (e.g., Freedman, Wilson and Madore 1991) is not critical in the present case. Instead, mean Vmagnitudes were obtained by calculating the intensity average for all data points with errors less than 0.3 msg. The photometry for the cosmic-ray-split frames was averaged prior to determining the average for the other independent epochs.

In the case 'of the *I* data, fewer phase points and hence a less uniform coverage with magnitude, are available to measure mean magnitudes. However, as the amplitudes of Cepheids scale as a function of wavelength (e.g., Freedman 1988), this property can be used to improve the estimates of the mean *I* magnitudes using additional knowledge from the *V* light curve. The ratio of *V* to *I* amplitude is almost identically equal to 2 to 1. (Freedman 1988 found ratios of 1.00:0.67:0.44:0.34 for B: V: R: I.) The mean *I* magnitudes were then computed as follows: In addition to the intensity mean based on all of the *V* data point's, another mean (intensity) *V* magnitude was calculated using only the epochs in common to both the *I* and *V* data sets for each star. The difference between the total mean *V* magnitude (based on 18 epochs) and the subset mean (based on epochs in common with *I*) was computed. This difference was then scaled by the *I* to *V* amplitude ratio, and applied as a correction factor to the *I*-band mean magnitude. 'l'he mean *V* and *I* magnitudes for the Cepheids are given in Tables 2 and 3. The offset corrections to the *I* magnitudes are given in the second-last column. The average absolute value of these corrections amounts to 0.06 msg. As in the case of the *V* photometry, only *I* data points with errors <0.3 mag were used in the calculation of the *I* intensity average.

5. THE DISTANCE TO M81

5.1 Period-luminosity Relations and Apparent Distance Moduli

V and *I* period-luminosity (PI,) relations for the 31 M81 Cepheids (denoted by open circles) are plotted in Figure 10. The M81 data are superimposed on the PI, relations for LMC Cepheids (solid dots) from Madore and Freedman (1991) based on data tabulated in Madore (1985). The solid lines are fits to the LMC data. The LMC PL relations adopted here are based only on a sample of 22 Cepheids having periods in the same range as the M81 Cepheids, that is with log P > 1.0. In addition, Cepheids with log P > 1.8 are excluded from the least-squares fits since both the evolutionary status and the reddening of these longer-period Cepheids are controversial.

We derive a distance to M81 adopting a true distance modulus to the LMC of 18.5 mag (*e.g.*, Feast and Walker 1987; Madore and Freedman 1991) and a mean total extinction to the LMC Cepheids of E(B- *V)* = 0.17 mag (e.g., see Bessel] 1991 for a recent review of LMC reddening). Centering the fits at the midpoint of the range of periods of the M81 sample, the following PI, relations at *V* and *I* are derived from the LMC sample:

$$M_V = -3.35(\pm 0.22)(\log P - 1.4) - 5.45\ (\pm 0.09)$$

$$M_I = -3.43(\pm 0.16)(\log P - 1.4) - 6.21\ (\pm 0.07)$$

The *rms* dispersion of the M81 PL relation about the above relation amounts to 0.35 at V and 0.30 at *I*. For the LMC sample the dispersion is ±0.31 at *V* and ±0.28 at *I*. The scatter in both the LMC and M81 samples are comparable: in fact, removing the 2 most discrepant points in the *V* PL relation (C8 and Cl O) decreases the scatter to 0.32, in even better agreement with the measured dispersion in the LMC sample. [C1O was found to be a double star (see the notes in Table 2), and C8 is one of tile faintest Cepheids discovered with < V > = 23.80 msg.] It should be

noted that these relations differ from those presented in Madore and Freedman (1991); the latter solutions were calculated over the range $0.2 < \log P < 1.8$.

The M81 apparent distance moduli are obtained by minimizing the residuals in the combined PL relations for the two galaxies, and determining the relative offset with respect to the I, MC. The apparent *relative* distance moduli between M81 and the LMC are measured to be 9.09 and 9.17 mag in *V* and *I*, respectively. 'l'he apparent distance moduli for M81 are then $\mu_V = 28.15$ and $\mu_I = 28.02$ mag (for our adopted values of $\mu_0 = 18.5$ and $E(B-V) = 0.17$ for the I, MC, with $A_V/E(B-V) = 3.30$ and $A_I/E(B-V) = 2.04$).

5.2 Extinction and True Distance Modulus

Before the true distance modulus to M81 can be determined, the *total* (foreground plus internal) extinction for the Cepheids must be accounted for. Measurements of the foreground Galactic extinction along the line of sight arc straightforward (for example, using multicolor photometry of bright, foreground stars or measuring the neutral hydrogen column density) and such corrections have been applied routinely to previous determinations of extragalactic distances; however, measuring the extinction internal to the parent galaxy is more difficult, and historically such corrections have not been applied. Multicolor photometry of neighboring field blue supergiants can yield an estimate of the general extinction (at least for the young supergiants in the vicinity of the Cepheids). However the WFC is not very sensitive in the blue and ultraviolet and thus such data for these intrinsically blue stars are not presently available. In any case, Cepheids are somewhat older objects than their blue main-sequence and supergiant progenitors, and the reddening derived for newly-formed OB stars more closely associated with dust, gas, and H II regions may not be directly applicable to the more widely distributed Cepheids.

The method that we have chosen to use yields a measure of the mean *total* extinction for

-the Cepheid sample itself. Previously this method has been applied to the Cepheids in IC 1613 (Freedman 1988), M33 (Freedman, Wilson and Madore 1991), M31 (Freedman and Madore 1990), and NGC 300 (Freedman *et al.* 1992). The procedure is to measure differential apparent distance moduli with respect to a well-studied sample of Cepheids in the Large Magellanic Cloud (LMC). Subsequently, a Galactic extinction law is fit to the differential apparent distance moduli as a function of inverse wavelength. The fit then yields a measure of the true distance modulus (at the λ^{-1} = O intercept) as well as the total difference in reddening with respect to the LMC sample.

The apparent *V* and *I* distance moduli for the M81 Cepheids have been fit to the Galactic extinction law of Cardelli, Clayton and Mathis (1 989) and the data are displayed in Figure 11. Photometry is available for 31 Cepheids at *V* and 25 Cepheids at *I*. For a true modulus to the LMC of 18.50 mag, the true distance modulus derived for M81 based on the total Cepheid sample is 27.80 ± 0.20 msg. An error budget for the determination of the distance is given in Table 7. A value of $E(B-V)$ = 0.11 mag is obtained for the mean total M81 extinction, assuming a value of $E(B-V)$ = 0.17 for the LMC.

An advantage of the above procedure is that the adopted LMC zero point and reddening are considered independently. As discussed by Freedman *et al.* (1992), in practice what is being measured is the *difference* between the total reddening of the LMC and, in this case, the M81 Cepheid sample. If, for example, a different extinction value of $E(B-V)_{LMC}$ = *0.10* (or 0.13) mag were to be preferred, the total M81 extinction becomes 0.04 (or 0.07) mag, but the difference in the extinction is fixed (at $E(B-V)_{M81}$ -- $E(B-V)_{LMC}$ = -0.06 mag), and the derived true distance modulus remains unaffected. Then, if a revision of the LMC distance zero point should ever be necessary in the future, the M81 modulus (and those of other galaxies) can be revised accordingly, independent of the absolute amoun of reddening in each system.

The distance derived above is based on the total observed sample of Cepheids (31 stars at

V and 25 stars at *I*). A number of tests were run to search for potential systematic errors in this modulus. Distance moduli were calculated for the following cases: (1) the sample of 25 stars having *both* *V* and *I* photometry, (2) only those Cepheids found on Chips 3 and 4 where the *I* calibration uncertainties are smaller, (3) only those stars described in the Notes to Tables 2 and 3 as isolated or having faint companions further than O'! 8 away, and (4) only for those Cepheids with periods greater than 15 days. In the latter case, (the longest-period Cepheids only) the *apparent* *V* and *I* moduli differed by 0.22 and 0.15 mag, respectively, whereas in the other 3 cases, the differences in the apparent moduli were $\leq$ 0.05. However, in *all* cases, the difference in the derived *true* distance moduli amounted to less than 0.05 msg.

Finally, potential systematic effects due to errors in the flat fields were searched for, in a similar manner to that described for the standard star calibration in §3.3. Use of the *Medium Deep Survey* flat field data revealed differences in the individual Cepheid magnitudes which reached 0.12 mag in *V,* and 0.09 mag in *I,* for stars near the edges of the frames. However, the apparent moduli in *V* and *I* changed by only -0.013 and -0.003 mag, respectively.

The determination of the true distance modulus to M81 in this paper is based solely on *VI* photometry, whereas the earlier studies using this method had four or more wavelengths available (generally *BVRI*). *1s* the *VI* photometry sufficient to obtain an accurate estimate of the reddening and the true distance modulus? This question can be addressed by examining the differences in distance moduli obtained based on *VI* and *BVRI* photometry for the galaxies for which all four wavelengths were available. Freedman, Wilson and M adore (1991) quote a value of 24.64 mag for the true distance modulus to M33 based on *BVRI* magnitudes. From *VI* photometry alone, they give 24.56 mag, or a difference of +0.08 msg. in the case of M31 (Freedman and Madore 1990), there are data available for three fields at different positions in the M31 disk. For these three independent data sets, the *BVRI* and *VI* solutions agree to within +0.01, +0.08 and 0.00 mag.

And for NGC 300 (Freedman *et al.* 1992), the *BVRI* and *VI* solutions differ by +0.04 msg. In all cases the total differences amount to less than 0.1 mag (which is thus less than 5% in distance). In addition, the estimates of the extinction from both the *BVRI* and *VI* photometry are also in good agreement. However we note that the differences, while small, are also systematic, and that closer distances are obtained from *VI* photometry alone. Still, we have independent reason to be confident that *VI* data alone are sufficient to obtain reliable values of the extinction and the true distance moduli at a level of approximately 5% in distance.

How much of the extinction estimated for the M81 Cepheids can be attributed to the extinction internal to M81? No previous estimate for the extinction of the M81 Cepheids has been available. Humphreys *et al.* (1986) estimated a value for M supergiants amounting to $A_v \sim 0.8 - 1.3$ msg. Based on Hα and radio continuum data, Kaufman *et al. (1987)* determined a value of $A_v \simeq 1.1 \pm 0.4$ mag for H 11 regions in M81. Burstein and Heiles (1984) give $A_B = 0.14$ ($E(B-V) = 0.035$) mag for the Galactic foreground extinction along the line of sight to M81. This small value for the Galactic foreground extinction suggests that the mean Cepheid reddening due to M81 alone amounts to $E(B-V) = 0.07$ mag ($A_v = 0.23$ mag for an assumed value of the total-to-selective extinction $R = 3.30$). This value is smaller than that inferred for the red supergiants and H 11 regions in M81. We note again however, that the exact amount of internal reddening appropriate for the M81 Cepheids depends on an accurate knowledge of the reddening of the LMC Cepheid sample. In addition, the mean reddening determined for the Cepheids cannot necessarily be generalized to other objects or other positions within M81, and vice versa.

Before concluding this section, we briefly comment on the potential effects of abundance on the Cepheid distance scale. The M81 distance determined above is with respect to the LMC; if there is a significant dependence of the 1'1, relation on abundance, a difference in metal licity between the M81 and LMC Cepheid samples could lead to a systematic error in the distance determination.

Recent calculations by Chiosi, Wood and Capitanio (1993) predict that the zero point of' the *I*-band Cepheid period-luminosity relation will differ by 0.1 mag for Cepheid samples having metallicities of $Z = 0.04$ and $Z = 0.001$.

Several efforts are currently being undertaken to address the metallicity question empirically. As part of the 11ST Key Project, we are undertaking a test in M101 for the effects of metallicity on the Cepheid period-luminosity relation, complementary to a similar test undertaken for M31 Cepheids (Freedman and Madore 1990). New 11 11 region abundances for all of the HST target galaxies have been measured (Zaritsky, Kennicutt, and Huchra 1993). Based on these data and published observations of M81 by Garnett and Shields (1987), abundances have been estimated for the two M81 11ST fields. For the Major Axis Field the [O/H] abundance is found to be a factor of 2.3 ± 0,5 times higher than the mean LMC abundance, and for the V30 Field the [O/H] abundance is found to be a factor of 1.5 ± 0.3 times higher than the J. MC. Assessing the effects of these differences in abundance will be deferred until the results of our M101 test are available. At this time we note that the results of Freedman and Madore (1990) suggest that the effects of metallicity on the true distance modulus will be small for differences of a factor of 2 at these observed abundances, with the effect on the true distance modulus determination amounting to less than $\pm 5\%$ *rms*. These results are consistent with the predictions of Chiosi, Wood and Capitanio (1993).

6. PREVIOUS DISTANCE ESTIMATES TO M81

There is a long history of attempts to measure the distance to M81. Despite an intensive ground-based observing program undertaken at the Palomar 5m by Hubble, Baade, Humason, Minkowski, Baum and Sandage, the discovery of Cepheids in M81 proved to be extremely difficult (e.g., see Baade, 1963; Sandage 1984). Ten variables were eventually confirmed, only two of which (V2 and V30) yielded well-determined periods, each of about 30 days (Sandage 1986, private communication). But no direct Cepheid modulus was initially determined for M81 based on these data; rather, on the basis of its assigned group membership (Holmberg 1950), M81 was *assumed* to be at the same distance as NGC 2403, its late-type spiral neighbor. The latter distance was determined on the basis of photographic photometry of Cepheids (Tammann and Sandage 1968) to be about 3.3 Mpc (μ = 27.6 mag).

Later, Sand age (1984) did return to the question of a direct Cepheid distance to M81. However, he simply argued that since the observed Cepheids in M81 are 0.8 mag fainter than the brightest Cepheids in NGC 2403, then M81 must be located further away. For an adopted value of μ^{AB}_{LMC} = 18.9 mag, corresponding apparent blue (AD) moduli of $\mu^{AB}_{NGC2403}$ = 27.9 and μ^{AB}_{M81} 28.8 mag were derived. The latter revised M81 distance amounts to 5.6 Mpc, almost a factor of two more distant than the previous assumed value. This larger apparent. distance modulus was then adopted in subsequent calibrations of H_0 (e. g., Sandage and Tammann 1984; Sandage 1988a, b; Tammann 1987). However, it should be noted that the *brightest* Cepheids in M81 are intermediate-period 30-day Cepheids while the brightest Cepheids in NGC 2403 are long-period (> 80-day) Cepheids. in fact, the two known 30-da.y Cepheids in M81have magnitudes comparable to those expected for 30-day Cepheids in NGC 2403 on the basis of its observed period-luminosity relation.

Subsequently, Freedman and Madore (198S) published CCD *I*-band photometry of the two known 30-day Cepheids based on data obtained at the Canada-France-Hawaii telescope (CFHT).

They determined an apparent modulus to M81 of μ_1 = 27.67 ± 0.09 msg. Correcting for Galactic foreground extinction, they derived a true distance modulus of μ_0=27.59 ± 0.31 msg. Madore, Freedman, and Lcc (1993) have recently compiled *BVRI* data obtained at the CFHT in January, 1988. These data are complementary to the results in the present paper, particularly since no B data have been obtained using HST. In addition, the *BVRI* data available for V2 and V30, although sparse, yield a true modulus of μ_0 = 27.79 ± 0.28 msg. These independent CCD observations agree WC]], to within the uncertainties, with the new determination of the distance to M81 based on the HST data.

The new distance to M81 presented in this study is in good agreement with several other recent distance estimates to this galaxy (for example, see the recent reviews by van den Bergh 1992; de Vaucouleurs 1993, in preparation). Van den Bergh quotes a mean distance modulus to M81 of 27.6 ± 0.15 mag based on four distance estimates; de Vaucouleurs presents a value based on the mean of eleven distance estimates and finds μ_0 = 27.78 ± 0.10 msg. The distance to M81 has been measured by using brightest stars and H 11 regions, the B and IR Tully-Fisher relation, Cepheids, the planetary nebula luminosity function, surface brightness fluctuations, and, (in this paper) HST observations of Cepheids. These measurements are summarized in Table 8. Except for Sandage's (1984) distance, which was based on a comparison of the magnitudes of brightest Cepheids, (see discussion in §6 above) all of the distances agree within their respective uncertainties. Because the distances are in basic agreement, the mean distance depends very little on how the data is weighted. The unwcightcd mean of these measurements, (excluding Sandage's distance) is 3.49 ± 0.16 Mpc.

7. SUMMARY AND DISCUSSION

The accurate measurement of H_0 and consequent definition of the scale size and age of the universe in absolute units remains to be carried out. The successful discoveries of Cepheids in M81 (this paper) and IC 4182 (Sandage *et al.* 1993) have demonstrated unequivocally that the Key Project is feasible and that accurate distances to nearby galaxies can be efficiently obtained using the HST.

With optimal power-law sampling, 31 Cepheids have been detected in M81 based on 18 epochs of *V* (F555W) observations. Despite the current spherical aberration of the primary mirror, the number of known Cepheids in M81 has been increased by over an order of magnitude. From these data, a true distance modulus has been obtained, corrected for the effects of interstellar reddening. The corresponding distance is 3.63 ± 0.34 Mpc.

With WFC2 currently scheduled for a December 1993 launch, the HST Extragalactic Distance Scale Key Project can be completed, and distances measured for ∼ 20 galaxies useful for calibrating a number of secondary distance methods. Currently, one of the largest uncertainties confronting the extragalactic distance scale is the small number of galaxies available to calibrate the secondary distance indicators. By calibrating several independent techniques, a firm determination of the systematic differences can be obtained, and the discrepancy in the distance scale in the region between 3 and 20 Mpc can be resolved. Our total error budget aims to provide a constraint on H_0 of 10%, while addressing potential systematic effects in both the Cepheid period-luminosity relation and in the various secondary methods, including potential errors due to the velocity field. A reliable value of H_0 now appears to be a realistic goal using the HST.

Acknowledgments

Support for this work was provided in part by NASA through grant numbers GO-227-87A. The ground-based calibration was funded in part by NSF grant AST-91-16496 to WI,]*'. JRM's work on the Tully-Fisher relation is supported by AST-91 -23646. BFM is supported in part by the NASA/IPAC Extragalactic Database (NED) and the Jet Propulsion Laboratory, Caltech. This research has made use of the NASA/IPAC Extragalactic Database (NED) which is operated by the Jet Propulsion Laboratory, Caltech, under contract with the National Aeronautics and Space Administration. We thank Rick Ebert, Booth Hartley, Gaylin Laughlin and other members of the Imaging Team at IPAC for their work in both developing and supporting the multi-purpose image- display package *Skyview.*

References

Aaronson, M., Mould, J., & Huchra, J. 1980, ApJ, 237, 655

Baade, W. 1963, in Evolution of Stars and Galaxies, (Harvard University Press, Cambridge, MA)

Bessell, M. S. 1991, AA, 242, L17

Bottinelli, 1,., Gouguenheim, I,., Paturel, G., and de Vaucouleurs, G. 1984, A&AS, 56,381

Burstein, D., & Heiles, C. 1984, ApJS, 54, 33

Cardelli, J. A., Clayton, G. C., & Mathis, J. S. 1989, ApJ, 345, 245

Chiosi, C., Wood, P. R., & Capitanio, N. 1993, ApJS, 86,541

Christian, C. A., Adams, M, Barnes, J. V., Butcher, H., Hayes, D. S., Mould, J. R., & Seigel, M., 1985 PAS]', 97, 363

de Vaucouleurs, G. 1978, ApJ, 224, 710

de Vaucouleurs, G., 1993, in preparation

Dressler, A., 1987, ApJ, 317, 1

Faber, S. M., Westphal, J. A., *et al.* 1991, WF/PC Orbital Science Verification Report

Feast, M., & Walker, A. R. 1987, ARA&A, 25, 345

Freedman, W. I,. 1988, APJ, 326, 691

Freedman, W. 1,., Grieve, G. R., & Madore, B. II'. 1985, ApJS, 59, 311

Freedman, W. I,., & Madore, B.F. 1988, ApJL, 332, 1,63

Freedman, W. I,., & Madore, 11.1'.1990, ApJ, 365, 186

Freedman, W. I,., Wilson, C. D., & Madore, B. F. 1991, ApJ, 372, 455

Freedman, W. 1,., *et al.* 1992, ApJ, 396, 80

Fukugita, M., Hogan, C. J, & Peebles, P. J. E. 1993, submitted to Nature.

Garnett D.R. & Shields, G.A. 1987, ApJ, 317, 82

Harris, H. C., Baum, W. A., Hunter, D. A., & Kreidl, T. J. 1991, AJ, 101, 677

Holmberg, E. E. 1950, Medd. Lunds Ohs., Ser. 2, No. 128

Hughes, S. M. G., *et al.*, 1993, in preparation

Humphreys, R. M., Aaronson, M., Lebofsky, M., McAlary, C. W., Strom, S. E. & Capps, R. W. 1986, AJ, 91, 808

Jacoby, G. H., Ciardullo, R., Ford, H. C., & Booth, J. 1989, ApJ, 344, 704

Kaufman, M., Bash, F. N., Kennicutt, R. C. & Hodge, 1'. W. 1987, ApJ, 319, 61

Kennicutt, R., *et al*, 1993, in preparation

Lafler, J. & Kinman, 1'.11.1965, ApJS, 11, 216

Lauer, T.R. 1989, PASP, 101, 445

Landolt, A. 1992, AJ, 104, 340

MacKenty *et* al. 1992, Wide Field and Planetary Camera instrument Handbook, Version 3.0, STScI Publications

Madore, B. II'., 1985, in IAU Colloquium 82, Cepheids: Theory and Observations,

cd. B.F. Madore (Cambridge: Cambridge University Press), p. 166

Madore, 11. F., & Freedman, W. L. 1991, I'ASI', 103, 933

Madore, B. F., & Freedman, W. 1,. 1994, in preparation

Madore, B.F., Freedman, W. I.. & Lee, M. G.1993, AJ, in preparation

McGonegal, R., McLaren, R. A., McAlary, C. W., & Madore, B. F., 1982, ApJ, 257, L33

Ritchie, C. E., & MacKenty, J. W. 1993, WF/PC nstrument Science Report 93-02, STScI Publications

Sandage, A. R. 984, AJ., 89, 621

Sandage, A. R. 988a, ApJ, 331,583

Sandage, A. R. 1988b, ApJ, 331,605

Sandage, A. R., Saha, A., '1'ammann, G. A., Panagia, N. & Macchetto, D. 1993, ApJL, 401, 1,7

Sandage, A. R. & Tammann, G. A.,. 1981, A Revised Shapley-Ames Catalog of Bright Galaxies, (Washington, D. C.: Carnegie Institution)

Sandage, A. R. & Tammann, G. A. 1984, Nature, 307, 326

Stellingwerf, R. F., 1978 ApJ 224,953

Stetson, P. 11.1987, I'ASI', 99, 101

Stetson, 1'. B. 1991a, in 3rd ESO/ST-ECF Data Analysis Workshop, held at Garching, 22-23 April 1991, ESO Conference and Workshop Proceedings No. 38, P.J. Grosbol and R.H. Warmels, eds., p.187

Stetson, 1'.11. 1991 b, in Astronomical Data Analysis Software and Systems 1, ASP Conference Series Vol. 25, D.M. Worrall, C. Biemesderfer, & J. Barnes, eds., p. 297

Stetson, 1'. 11., 1993, in preparation

Tammann, G. A., 1987, in Observational Cosmology, IAU Symposium No. 124, (eds. A. Hewitt, G. Burbidge & 1,. Z. Fang), (Dordrecht: Reidel), p. 151

Tammann, G. A., & Sandage, A. R. 1968, ApJ., 151, 825

Tonry, J. L., 1991, ApJ, 373, L1

van den Bergh, S., 19,92, I'ASI', 104, 861,

Welch, 1). 1,. & Stetson,]'. 11.1993, AJ, 105, 1813

Wisnewski, W. Z., & Johnson, H. L. 1968, Comm. Lunar Planet. Lab., No. 112

Zaritsky D., Kennicutt R. C., & Huchra, J.]'. 1993, ApJ, submitted

Figure Captions

Fig. 1 -- Sampling variance of light curves for a) data taken using the optimal strategy adopted for the HST program and b) data taken at uniformly-spaced intervals. The plot is normalized such that low values indicate uniform sampling was achieved, and high values indicate clumping and redundancies in the actual realization. For the optimally sampled case a), the twelve data points were chosen to fall within the same 45-day window, but to have a similar variance over that window. Note that the mean variance in the 45-day window is very close to flat, and shows significantly smaller variations as compared to the uniform spacing of case b).

Fig. 2 – (a) An illustration of the best sampling for the optimal sampling frequency shown in Figure lb. (b) The worst sampling for the optima] sampling frequency shown in Figure 1 b.

Fig. 3 – A reproduction of a *B* plate of M81 taken at the prime focus of the *CFHT*. The areas marked corresponds to the fields observed by HST in this Cepheid discovery program. North is approximately at the top, east to the left; the exact orientation is shown. The seeing during this exposure was about O'! 5 and the exposure time was 2 hours.

Fig. 4 – a-d) Reproductions of the 4 WFC V-band median-filtered images for the 'Major Axis Field'). The 4 WFC chips all have different relative orientations which are labeled on the plots.

Fig. 5- a-d) Same as Figure 4 for the 'V30 Field'.

Fig. 6 – Finder charts for all of the Cepheids listed in Tables 2 and 3. The position of each Cepheid is marked. The greyscale mapping for each field is set independently so that each Cepheid can be clearly identified. The finder charts cover an area of 5" x5".

Fig. 7a-f – Light curves of the M81 'Major Axis Field' Cepheids phased to the periods listed in Table 2 for Chips 1-4.

Fig. **8a,b** - Light curves of the MS] 'V30 Field' Cepheids phased to the periods listed in 'l'able 3 for Chips 1-4.

Fig. 9- Phased light curve for the eclipsing variable found in the M81 'Major Axis Field'.

Fig. 10 **a,b**– a) V-band period luminosity relation for 3 M81 Cepheids (open circles) plotted with respect to the LMC Cepheid data (solid dots) shifted by 9.09 mag in apparent modulus. b) *I*-band period luminosity relation for 25 M81 Cepheids (open circles) plotted with respect to the LMC Cepheid data (solid dots), shifted by 9.17 mag in apparent modulus.

Fig. 11– Apparent distance modulus as a function of inverse wavelength. The dashed line illustrates the Galactic extinction law of Cardelli, Clayton and Mathis (1 989) for $E(B-V) = 0.11$ msg. The true distance modulus is given by the intercept in this plot and amounts to 27.80 msg.

Table 1: Calibration of WFC ALLFRAME Photometry in M81

	$V - F555W_{ALLFRAME}$		$F785LP - F785LP_{ALLFRAME}$		N
	Ground-based	IDT Report	Ground-based	IDT Report	
Chip 1	3.45 ± 0.04	(3.51)	2,56 ± 0.13	(2.70)	14
Chip 2	3.62 ± 0.05	(3.68)	2.72 ± 0.10	(2.73)	14
Chip 3	3.63 ± 0.03	(3.66)	2.71 ± 0.05	(2.59)	22
Chip 4	3.54 ± 0.04	(3.57)	2.80 ± 0.04	(2.59)	23

'1'able 2: Properties of the M81 Major Axis Cepheids

ID	x	y	P (days)	$< V >$	$< I >$	$\Delta < I >$	N_{sig}
Chip 1							
c l	57.06	426.08	20.5	23.67	22.56	–0.05	1.4
C2	115.00	457.62	19.6	23.46	22.42	–0.08	1.8
C3	88.84	701.58	17.5	22.88	22.05	4-0.04	2.0
C4	729.84	83.62	15.7	23,40			1.4
C5	104.72	455.44	10.7	23.44	22.58	–0.09	2.1
Chip 2							
C6	25.12	374.87	40.8	22.26	21.36	+0.08	4.0
C7	49.28	418.93	27.2	22.60	21.69	+0.05	3.8
C8	492.22	137.77	24.6	23.80	22.30	–0.03	3.9
C9	202.38	545.89	14.7	23.11	22.13	+0.05	2.3
C10	29.58	416.31	12.8	22.91	22.29	+0.01	2.5
Chip 3							
C11	258.93	90.46	47.2	22.46	21.30	+0.11	2.8
C12	507.05	536.98	23.7	22.63	21.88	+0.02	3.5
C13	155.09	69.98	18.6	23.56	22.75	+0.06	1.4
C14	242.09	694.86	12.7	23.54	22.57	–0.02	1.5
C15	172.22	126.11	11.2	23.84	22.96	–0.23	1.8
C16	384.50	4.16	10.9	23.54			2.2
Chip 4							
C17	26.58	568.19	45.9	21.68	20.89	+0.01	2.7
C18	162.34	529.96	36.7	22.47	21.47	–0.02	2.7
C19	365.13	660.03	23.6	23.30	22.45	+0.01	2.7
C20	553.48	412.85	17.0	23.21	22.41	–0.21	2.3
C21	530.02	456.26	14.2	23.25	22.66	+0.08	3.0
C22	347.93	415.94	13.6	23.20	22.12	–0.07	2.8
C23	333.11	48.24	11.7	23.56	22.72	–0.13	1.6
C24	14.13	414.94	11.5	23.42			1.6

Notes:

Cl: isolated; very noisy I light curve

C2: in crowded region with brighter companion

C3: isolated

C4: close brighter companion, P = 14.5 days is also good

C5: in crowded region with brighter companion; very noisy I light curve

C6: brightest star in crowded region; close companion; 1' = 52.1 days is also good

C7: nearby companion (~ 0.7 arcsec)

C8: isolated

C9: close, fainter companion

Cl O: double (two stars found) in crowded region
C11: wry faint nearby companion
Cl 2: companion stars ~ 0.8 – 1.0 arcsec away
C1 3: in crowded region, 1' = 16.9 days is also goOd
Cl 4: very faint nearby companions; very noisy Ilight curve, dots not phase well
Cl 5: brightest star in crowded region
C16: close companion; near frame edge, therefore only 16 data points
Cl 7: elongated image
C18: isolated; very faint nearby companions
C19: brightest star in crowded region; very noisy I light curve, does not phase well
C20: isolated
C21: fainter close companion ~ 0.3 arcsec away; P = 13.7 days is also gOOd
C22: faint companion ~ 0.7 arcsec away
C23: isolated; nearest companion ~ 0.8 arcsec away; very noisy Ilight curve
C24: very faint close companion (~ 0.4 arcsec)

Table 3: Properties of the M81 V30 Field Cepheids

ID	x	y	P (days)	< v >	< 1 >	$\Delta < I >$	N_{sig}
Chip 2							
C25	720.59	420.45	17.4	23.58			1.2
Chip 3							
C26	245.42	161.03	54.8	21.78	20.64	0.00	1.7
C27	14.95	328.28	30.0	22.38			2.2
C28	419.38	254.39	27.6	22.62	21.66	–0.03	2.0
Chip 4							
C29	174.32	480.87	30.0	22.39	21.32	–0.02	2.2
C30	625.83	327.24	18.1	23.04	22.23	+0.03	1.7
C31	506.31	256.03	14.9	23.17			1.8

Notes:
C25: isolated
C26: elongated image; nearby companion
C27: isolated: also known as V30
C28: nearby companion
C29: elongated image
C30: isolated; very noisy I light curve
C31: nearby companions

Table 4: V Photometry of M81 Cepheids

JD + 2400000	V	σ_V	JD + 2400000	V	σ_V
C1	P = 20.5		C2	P = 19.6	
48620.600	23.79	0.26	48620.600	23.21	0.13
48620.612	23.79	0.21	48620.612	23.16	0.12
48621.536	23.83	0.30	48621.536	23.14	0.08
48630.493	23.36	0.13	48630.493	23.91	0.15
48641.213	23.87	0.17	4/3641.213	23.31	0.11
48641.956	24.09	0.23	48641.956	23.35	0.17
48643.224	23.99	0.23	48643.224	23.38	0.14
48644.567	23.89	0.20	48644.567	23.47	0.07
48646.365	24.00	0.36	48646.365	23.62	0.19
48646.377	24.33	0.29	48646.377	23.61	0.27
48649.188	23.91	0.14	48649.188	23.86	0.18
48653.136	23.31	0.15	48653.136	23.31	0.58
48653.148	23.12	0.14	48653.148	23.69	0.25
4865'7.704	23.34	0.13	48657.704	23.03	0.10
48662.852	24.10	0.25	48662.852	23.32	0.11
48662.864	23.85	0.20	48662.864	23.40	0.14
48984.166	23.17	0.12	48984.167	24.01	0.19
48987.246	23.52	0.16	48987.246	24.13	0.23
48992.272	24.06	.069	48992.272	23.08	0.14
49000.029	23.91	0.20	49000.029	23.74	0.17
49012.208	24.00	0.28	49012.208	23.15	0.15
49029.177	23.64	0.19	49029.177	24.01	0.21
C3	P = 17.5		C4	P = 15.7	
48620.600	23.46	0.19	48620.600	23.16	0.15
48620.612	23.71	0.30	48620.612	23.06	0.20
48621.536	23.33	0.15	48621.536	23.48	0.28
48630.493	22.78	0.13	48630.493	23.59	0.20
48641.213	23.26	0.12	48641.213	23.72	0.30
48641.956	23.05	0.18	48641.956	23.86	0.24
48643.224	22.62	0.08	48643.224	23.92	0.33
48644.567	22.59	0.09	48644.567	23.77	0.21
48646.365	22.84	0.13	48646.365	23.57	0.28
48646.377	22.83	0.14	48646.377	23.95	0.24
48649.188	23.08	0.23	48649.188	22.95	0.16
48653.136	23.29	0.16	48653.136	23.13	0.19
48653.148	23.36	0.25	48653.148	23.25	0.21
48657.704	22.95	0.51	48657.704	23.84	0.23
48662.852	22.62	0.09	48662.852	23.01	0.17
48662.864	22.72	0.11	48662.864	23.04	0.14
48984.166	23.19	0.11	48984.166	23.23	0.55
48987.246	23.38	0.21	48987.246	23.88	0.29
48992.272	22.87	0.13	48992.272	23.62	0.19
49000.029	22.91	0.10	49000.029	23.70	0.30
49012.208	22.48	0.18	49012.208	23.08	0.11
49029.177	22.45	0.09	49029.177	23.25	0.23

Table 4- Continued

.11) + 2400000	V	σ_V	JD + 2400000	V	σ_V
C5	P = 10.7		C6	P = 40.8	
48620.000	23.95	0.29	48620.600	22.65	0.11
48620.612	24.05	0.43	48620.612	22.81	0.13
48621.536	23.97	0.26	48621.536	22.79	0.08
48630.493	23.99	0.20	48630.493	21.79	0.07
48641.213	23.91	0.21	48641.213	21.99	0.07
48641.956	24.25	0.35	48641.956	21.94	0.08
48643.224	23.62	0.15	48643.224	22.04	0.07
48644.567	23.22	0.13	48644.567	22.04	0.06
48646.365	23.04	0.16	48646.365	22.09	0.07
48646.377	23.15	0.19	48646.377	22.21	0.07
48649.188	23.32	0.11	48649.188	22.18	0.09
48653.136	23.91	0.21	48653.136	22.43	0.08
48653.148	24.02	0.25	48653.148	22.33	0.07
48657.704	23.21	0.11	48657.704	22.53	0.08
48662.852	23.81	0.21	48662.852	22.69	0.12
48662.864	23.57	0.18	48662.864	22.63	0.09
48984.166	23.77	0.26	48984.166	22.58	0.08
48987.246	23.30	0.13	48987.246	22.66	0.10
48992.272	23.99	0.13	48$)92.272	22.79	0.12
49000.029	22..55	0.26	49000.029	21.67	0.11
49012.208	23.59	0.12	49012.208	22.18	0.06
49029.177	23.23	0.14	49029.177	22.77	0.11
C7	P = 27.2		C8	P = 24.6	
48($20.600	22.76	0.14	48620.600	23.63	0.15
48620.612	22.72	0.11	48620.612	23.63	0.12
48621.536	22.77	0.08	48621.536	23.22	0.06
48630.493	23.18	0.09	48630.493	23.71	0.16
48641.213	22.33	0.09	48641.213	24.40	0.20
48641.956	22.18	0.08	48641.956	24.24	0.25
48643.224	22.49	0.07	48643.224	21.22	0.52
48644.567	22.43	0.09	48644.567	23.86	0.15
48646.365	22.69	0.0's	48646.365	23.10	0.10
48646.377	22.66	0.10	48646.377	23.21	0.11
48649.188	22.85	0.11	48649.188	23.44	0.12
48653.136	23.14	0.12	48653.136	23.60	0.16
48653.148	23.16	0.12	48653.148	23.58	0.13
48(557.704	23.30	0.11	48657.704	24.02	0.15
48662.852	22.00	0.06	48662.852	24.23	0.20
48662.864	22.05	0.10	48662.864	24.22	0.18
48984.166	22.94	0.07	48984.166	24.13	0.16
48987.246	22.25	0.08	48987.246	24.16	0.20
48992.272	22.22	0.10	48992.272	23.50	0.13
49000.029	22.62	0.09	49000.029	23.91	0.13
49012.20S	23.08	0.16	40012.208	24.11	0.15
49029.177	22.73	0.10	49029.177	24.38	0.20

Table 4 Continued

JD + 2400000	V	σ_V	JD + 2400000	V	σ_V
C9	P = 14.7		C10	P = 12.8	
48620.600	23.15	0.14	48620.600	23.29	0.14
48620.612	23.28	0.12	48620.612	23.34	0.14
48621.536	23.23	0.12	48621.536	23.48	0.13
48630.493	23.22	0.10	48630.493	22.94	0.08
48641.213	23.51	0.19	48641.213	22.60	0.06
48641.956	23.62	0.14	48641.956	22.86	0.07
48643.224	23.56	0.14	48643.224	22.85	0.14
48644.567	23.34	0.12	48644.567	23.10	0.08
48646.365	22.60	0.08	48646.365	23.22	0.15
48646.377	22.57	0.12	48646,377	22.98	0.12
48649.188	23.11	0.12	48649.188	23.44	0.14
48653.136	23.35	0.37	48653.136	22.48	0.09
48653.148	23.46	0.12	48653.148	22.50	0.14
48657.704	23.50	0.11	48657.704	23.20	0.44
48662?.852	22.86	0.07	48662.852	23.34	0.12
48662.864	22.76	0.09	48662.864	23.02	0.33
48984.166	22.78	0.21	48984.166	23.03	0.08
48987.246	22.86	0.19	48987.246	22.80	0.09
48992.272	23.58	0.14	48992.272	23.46	0.15
49000.029	22.73	0.18	49000.029	22.58	0.06
49012.208	23.41	0.30	49012.208	22.41	0.10
49029.177	22.73	0.12	49029.177	22.87	0.08
C11	P = 47.2		C12	P = 23.7	
48620.600	22.33	0.11	48620.600	22.39	0.08
48620.612	22.17	0.06	48620.612	22.43	0.11
48621.536	22.17	0.09	48621.536	22.44	0.08
48630.493	22.08	0.08	48630.493	23.01	0.10
4S641.213	22.44	0.11	48641.213	22.19	0.06
48641.956	22.38	0.07	48641.956	22.22	0.10
48643.224	22,40	0.07	48643.224	22.31	0.08
48644.567	22,50	0.08	48644.567	22.37	0.07
48646.365	22.25	0.30	48646.365	22.55	0.08
48646.377	22.35	0.08	48646.377	22.00	0.50
48649.188	22.61	0.10	48649.188	22.71	0.09
48653.136	22.71	0.08	48653.136	23.13	0.07
48653.148	22.80	0.09	48653.148	23.08	0.09
48657.704	22.79	0.08	4865'7.704	23.10	0.10
48662.852	2.2.81	0.09	48662.852	22.25	0.09
48662.864	22.91	0.09	48662.864	22.30	0.10
48984.166	22.74	0.08	48984.166	22.98	0.11
48987.246	22.86	0.13	48987.246	23.06	0.12
48$)92.2272	22.80	0.14	48992.272	23.16	0.10
49000.029	21.97	0.09	49000.029	22.49	0.06
49012.208	22.26	0.09	49012.208	23.20	0.08
49029.177	22.66	0.07	49029.177	22.77	0.08

Table 4 Continued

JD + 2400000	V	σ_V	JD + 2400000	V	σ_V
C13	P = 18.6		C14	P = 12.7	
48620.600"	23.74	0.31	48620.600	23.80	0.23
48620.612	24.18	0.34	48620.612	23.80	0.21
48621.536	23.94	0.18	48621.536	23.77	0.16
48630.493	23.30	0.23	48630.493	23.42	0.12
48641.213	23.70	0.21	48641.213	23.24	0.11
48641.956	23.61	0.18	48641.956	23.28	0.17
48643.224	23.6'7	0.15	48643.224	23.58	0.13
48644.567	23.26	0.15	48644.567	23.40	0.22
48646.365	23.48	0.17	48646.365	23.90	0.17
48646.377	23.2'7	0.14	48646.377	23.96	0.19
48649.188	23.51	0.19	48649.188	23.72	0.13
48653.136	23.85	0.18	48653.136	23.09	0.08
48653.148	23.65	0.22	48653.148	23.31	0.13
48657.704	23.79	0.19	48657.704	23.70	0.16
48662.852	23.32	0.13	48662.852	23.47	0.10
48662.864	23.26	0.16	48662.864	23.64	0.20
48984.166	23.40	0.11	48984.166	23,27	0.14
48987.246	23.63	0.18	48987.246	23.69	0.15
48992.272	24.11	0.30	48992.272	23.57	0.11
49000.029	23.31	0.12	49000.029	23.53	0.13
49012.208	24.03	0.34	49012.208	23.61	0.13
49029.177	23.72	0.25	49029.177	23.77	0.15
C15	P = 11.2		C16	P = 10.9	
48620.600	23.56	0.16	48620.600	23.18	0.14
48620.6)2	23.63	0.18	48620.612	23.14	0.12
48621.536	23.33	0.14	48621.536	23.22	0.12
48630.493	24.31	0.27	48630.493	23.66	0.17
48641.213	23.87	0.25	48641.213	23.6S	0.10
48641.956	24.05	0.23	48641.956	23.41	0.11
48643.224	23.82	0.18	48643.224	23.25	0.11
48644.567	23.26	0.09	48644.567	23,62	0.16
48646.365	23.61	0.14	48646.365	23.85	0.16
48646.377	23.76	0.12	48646.377	23.81	0.13
48649.188	24.22	0.23	48649.188	24.07	0.17
48653.136	24.07	0.19	48653.136	23.36	0.12
48653.148	23.94	0.18	48653.148	23.22	0.10
48657.704	23.53	0.17	48657.704	23.98	0.13
48662.852	24.31	0.26	48662,852	23.71	0.14
48662.864	2.4.07	0.19	48662.864	23.88	0.19
48984.166	23.97	0.15			
48987.246	24.26	0.30			
48992?.272	23.43	0.12			
49000.02.9	24.42	0.24			
49012.208	24:29	0.29			
49029.177	23.90	0.10			

Table 4- Continued

JD + 2400000	V	σ_V	JD + 2400000	V	σ_V
C17	P = 45.9		C18	P = 36.7	
48620.600	21.50	0.10	48620.600	22.28	0.10
48620.612	21.51	0.10	48620.612	22.23	0.12
48621,536	21.50	0.09	48621.536	22.32	0.11
48630.493	21.76	0.12	48630.493	22.64	0.11
48641,213	21.85	0.38	48641.213	22.82	0.16
48641.956	21.68	0.13	48641.956	22.93	0.11
4s643.124	21.96	0.09	48643.224	22.98	0.14
48644.567	21.95	0.08	48644.567	22.79	0.10
48646.365	22.00	0.10	48646.365	22.85	0.18
48646.377	22.00	0.13	48646.377	22.76	0.09
48649.188	22.00	0.12	48649.188	22.38	0.08
48(353.136	20.49	0.45	48653.136	22.15	0.13
48653.148	21.92	0.08	48653.148	22.04	0.10
48657,704	21.70	0.11	4865'7.704	22.22	0.10
48662,852	21.44	0.09	48662.852	22.37	0.09
48662.864	21.38	0.08	48662.864	22.38	0.10
48984.166	21.43	0.09	48984.166	22.13	0.07
4s987.246	21.53	0.09	48987.246	22.22	0.06
48992,272	21.64	0.06	48992.272	22.39	0.09
49000.029	21.71	0.10	49000.029	22.62	0.09
49012.208	21.98	0.08	49012.208	22.83	0.08
49029.177	21.44	0.11	49029.177	22.35	0.10
C19	P = 23.6		C20	P = 17.0	
48620.600	23.60	0.19	48620.600	23.04	0.09
48(320.612	23.70	0.27	48620.612	22.84	0.14
486?1.536	23.92	0.17	48621.536	22.85	0.12
48630.493	22.92	0.14	48630.493	23.70	0.15
48641.213	23.47	0.14	48641.213	23.39	0.19
48641.95(5	23.58	0.17	48641.956	23.28	0.0s
48643.224	23.54	0.13	48643.224	23.73	0.22
48644.567	23.97	0.18	48644.567	23.63	0.16
48646.365	23.97	0.20	48646.365	23.75	0.31
48646.377	23.92	0.23	48646.377	23.66	0.19
48649.188	23.82	0.15	48649.188	23.57	0.15
48653.136	22.78	0.13	48653.136	22.80	0.07
48653.148	22.73	0.10	48653.148	22.73	0.17
48657.704	23.20	0.16	48657.704	23.10	0.13
48662.852	23.28	0.13	48662.852	23.74	0.19
48662.864	23.37	0.14	48662.864	23.87	0.25
48984.166	22.91	0.08	48984.166	23.55	0.14
48987.246	22.75	0.27	48987.246	23.65	0.39
48992.2?72	23.28	0.09	48992.272	22.81	0.19
49000.029	23.86	0.21	49000.029	23.36	0.11
49012.208	23.10	0.15	49012.208	22.96	0.10
49029.177	22.83	0.10	49029.177	22.89	0.11

Table 4- Continued

JD + 2400000	V	σ_V	JD + 2400000	V	σ_V
C21	P = 14.2		C22	P = 13.6	
486'20.600	23.82	0.33	48620.600	23.26	0.08
48620.612	23.88	0.14	48620.612	23.50	0.15
48621.536	23.55	0.11	48621.536	23.48	0.13
48630,493	23.08	0.11	48630.493	23.05	0.12
48641,213	24.08	0.21	48641.213	22.88	0.11
48641.956	23.80	0.13	48641.956	22.91	0.08
4s643,224	22.81	0.11	48643.224	23.10	0.15
48644.567	23.22	0.09	48644.567	23.31	0.11
48646.365	23.44	0.15	48646.365	23.38	0.14
48646.377	23.48	0.21	48646.377	21.75	0.51
48649.188	23.50	0.11	4.S64$).188	23.52	0.)4
48653.136	24.08	0.26	4S653.136	22.79	0.10
48653.148	24.03	0.20	48653.148	22.76	0.13
48657.704	22.83	0.09	48657.704	23.11	0.09
48662.852	23.56	0.08	48662.852	23.55	0.15
48662.864	23.38	0.13	48662.864	23.64	0.24
48984.166	23.17	0.08	48984.166	23.20	0.16
48987.246	23.10	0.13	48987.246	23.56	0.12
48992.272	23.74	0.17	48992.272	22.98	0.13
49000.029	22.51	0.20	49000.029	23.38	0.14
49012.208	23.65	0.14	49012.208	23.15	0.10
49029.177	22.78	0.09	49029.177	23.55	0.11
C23	P = 11.7		C24	P = 11.5	
48620.600	23.64	0.19	48620.600	23.21	0.15
48620.612	23.32	0.12	48620.612	23.14	0.21
48621.536	23.65	0.29	48621.536	23.80	0.32
48630.493	23.46	0.22	48630.493	23.15	0.14
48641.213	23.00	0.13	48641.213	23.73	0.24
48(541.956	23.36	0.21	48641.956	23.08	0.18
48643.224	23.40	0.17	48643.224	23.39	0.13
48044.567	23.72	0.23	48644.567	23.48	0.12
48646,365	23.79	0.22	48646.365	23.77	0.42
48646.377	23.64	0.41	48646.377	23.58	0.30
48649.188	24.17	0.18	48649.188	24.30	0.33
48653.136	23.00	0.14	48653.136	23,47	0.27
48653.148	23.15	0.12	48653.148	23.37	0.18
48657.704	23.70	0.18	48657.704	23,56	0.20
48(X2.852	23.61	0.21	48662.852	23.81	0.26
48662.$64	23.84	0.22	48662.864	24.01	0.31
48984.166	24.00	0.19	48984.166	24.19	0.23
48987.246	24.22	0.39	48987.246	23.48	0.29
48992,272	23.50	0.10	48992.272	23.85	0,31
49000.029	23.96	0.29	49000.029	23.33	0.22
49012.208	23.91	0.29	49012.208	23.21	0.61
49029.177	23.56	0.10	49029.177	24.98	0.51

Table 4 Continued

JD + 2400000	V	σ_V	JD + 2400000	V	σ_V
C25	1' = 17.4		C26	1' = 54.8	
48620.867	23.10	0.45	48620.867	22.10	0.16
48620.879	23.67	0.37	48620.879	22.21	0.13
48621.803	23.43	0.24	48621.803	22.08	0.13
48630.759	24.14	0.46	48630.759	21.51	0.13
48641.150	24.11	0.36	48641.150	21.62	0.13
48642.025	23.96	0.30	48642.025	21.58	0.13
48643.098	24.15	0.39	48643.098	21.62	0.14
48644.633	24.29	0.41	48644.633	21.64	0.14
48646.231	24.06	0.46	48646.231	21.64	0.15
48646.243	24.30	0.54	48646.243	21.66	0.14
48649.062	24.52	0.46	48649.062	21.68	0.13
48653.002	23.16	0.22	48653,002	21.s1	0.15
48653.014	23.32	0.19	48653.014	21.77	0.12
48658.106	23.85	0.29	48658.106	21.89	0.12
48663.053	24.31	0.56	48663.053	21.91	0.16
48663.065	24.52	0.38	48663.065	21.97	0.13
48984.101	23.25	0.24	48984.101	21.93	0.15
48987.380	23.71	0.26	48987.380	21.34	0.39
48992.334	24.09	0.25	48992.334	22.09	0.16
49000.162	23.46	0.19	49000.162	22.32	0.13
49012.273	24.27	0.40	4$)012.273	21.54	0.13
49029.241	23.98	0.38	49029.241	21.65	0.13
C27	P = 30.0		C28	P = 27.6	
48620.867	22.67	0.18	48620.867	22.69	0.15
48620.879	22.65	0.16	48620.879	22.73	0.15
48621.803	22.81	0.18	48621.803	22.76	0.14
48630.759	22.91	0.19	48630.759	23.04	0.18
48641.150	21.92	0.19	48641.150	22.21	0.15
48642.025	22.06	0.15	48642.025	22.15	0.16
48643.098	22.18	0.15	48643.098	22.35	0.16
48644.633	22.17	0.19	48644.633	22.48	0.14
48646.231	22.26	0.20	48646.231	22.57	0.15
48646.243	22.25	0.22	48646.243	22.61	0.16
48649.062	22.42	0.19	48649.062	22.65	0.13
48653.002	22.90	0.18	48653.002	22.93	0.22
48653.014	22.74	0.17	48653.014	22.97	0.21
48658.106	22.70	0.16	48658.106	23.04	0.19
48(363.053	21.44	0.47	48663.053	23.30	0.23
48663.065	22.87	0.18	48663.065	23.23	0.19
48984,101	22.78	0.19	48984.101	22.89	0.16
48987.380	22.74	0.18	48987.380	23.03	0.17
48992.334	22.89	0.15	48992.334	22.95	0.20
49000."162	21.94	0.13	49000.162	22.20	0.15
49012.273	22.58	0.15	49012.273	22.85	0.14
49029.241	21.76	0.15	49029.241	22.19	0.14

JD + 2400000	V	σ_V	JD + 2400000	V	σ_V
C29	P = 30.0		C3◦	= 8.1	
48620.867	22.26	0.10	48620.867	23.34	0.25
48620.879	22.06	0.18	48620.879	23.03	0.22
48621.803	22.31	0.13	48621.803	23.12	0.32
48630.759	22.68	0.17	48630.759	22.23	0.16
48641.150	23.10	0.18	48641.150	23.59	0.26
48642.025	23.05	0.19	48642.025	23.72	0.22
48643.098	23.14	0.23	48643.098	23.47	0.24
48644.633	22.71	0.45	48644.633	23.38	0.22
48646.231	22.85	0.18	48646.231	23.20	0.23
48646.243	23.03	0.20	48646.243	23.34	0.20
48649.062	21.83	0.12	48649.062	21.99	0.98
48653.002	22.04	0.14	48653.002	23.00	0.21
48653.014	22.13	0.11	48653.014	22.79	0.19
48658.106	22.19	0.12	48658.106	23.31	0.19
48663.053	22.65	0.21	48663.053	23.26	0.24
48663.065	22.40	0.14	48663.065	23.20	0.23
48984.101	22.10	0.13	48984.101	23.34	0.24
48987.380	22.23	0.13	48987.380	23.41	0.26
48992.334	22.39	0.14	48992.334	22.29	0.15
49000.162	22.70	0.18	49000.162	23.10	0.16
49012.273	22.05	0.12	49012.273	22.67	0.17
49029.241	23.00	0.51	49029.241	22.38	0.48

C3	P = 14.9	
48620.867	22.98	0.18
48620.879	22.95	0.22
48621.803	22.65	0.20
48630.759	23.60	0.25
48641.150	23.18	0.24
48642.025	23.20	0.24
48643.098	23.30	0.25
48644.633	23.48	0.28
48646.231	23.87	0.39
48646.243	24.62	0.65
48649.062	23.42	0.22
48653.002	22.69	0.21
48653.014	22.79	0.17
48658.106	23.30	0.22
48663.053	23.59	0.24
48663.065	23.82	0.27
48984.101	23.06	0.17
48987.380	23.54	0.22
48992.334	23.39	0.21
49000.162	23.18	0.22
49012.273	22.81	0.17
49029.241	23.03	0.18

Table 5: 1 Photometry of M81 Cepheids

JD + 2400000	I	σ_I	JD + 2400000	I	σ_I
C1	P = 20.5.		C2	P = 19.6	
48630.549	22.48	0.21	48630.549	22.73	0.15
48643.2S0	22.84	0.12	48643.280	22.29	0.15
48649.244	22.89	0.32	48649.244	22.67	0.24
48662.920	22.46	0.14	48662.920	22.37	0.18
49000.085	22.70	0.27	48$)87.302	23.39	0.72
			49000.085	22.52	0.13
C3	P = 17.5		C4	P = 15.7	
48630.549	22.06	0.17	48630.549	23.11	0.47
48643.280	21.96	0.14	48643.280	23.44	0.47
48649.244	22.01	0.13	48662.920	22.76	0.32
48662.920	21.86	0.15	489 S7.302	23.17	0.39
49000.085	22.14	0.10	49000.085	22.70	0.19
C5	P = 10.7		C6	P = 40.8	
48630.549	23.10	0.29	48630.549	21.08	0.12
48643.280	22.27	0.31	48643.280	21.13	0.06
48649.244	22.41	0.29	48649.244	21.37	0.07
48662.920	22.62	0.22	48662.920	21.72	0.08
48987.302	22.04	0.98	48987.302	21.49	0.14
490 00.085	22.87	0.89	49000.085	21.03	0.08
C7	P = 27.2		C8	P = 24.6	
48630.549	22.00	0.13	48630.549	22.32	0.15
48643.280	21.51	0.08	48643.280	22.91	0.22
48649.244	21.93	0.10	48649.244	22.10	0.17,
48662.920	21.36	0.10	48662.920	22.55	0.22
48987.302	21.49	0.25	48987.302	22.50	0.21
49000.085	21.69	0.10	49000.085	22.26	0.16
C9	P = 14.7		C10	P = 12.8	
4S630.549	22.25	0.18	48630.549	22.27	0.12
48643.280	22.55	0.19	48643.280	22.28	0.11
48649.244	22.06	0.11	48649.244	22.75	0.23
48662.920	21.94	0.12	48662.920	22.91	0.11
48987.302	21.92	0.13	48987.302	22.00	0.20
49000.085	21.92	0.13	49000.085	22.21	0.16

Table 5 Continued

JD + 2400000	I	σ_I	JD + 2400000	I	σ_I
C11	P = 47.2		C12	P = 23.7	
4s630.549	21.12	0.10	48630.549	21.97	0.08
4s643,280	21.27	0,06	48643.280	21.79	0.08
48649.244	21.40	0.22	48649.244	21.80	0.09
48662.920	21.37	0.67	48662.920	21.74	0.12
4{)000.085	21.02	0.09	489 S7.302	22.29	0,13
			49000.085	21.71	0.08
C13	P = 18.6		C14	P = 12.7	
48030.549	21.78	0.41	48630.549	22.53	0.15
48643.280	22.53	0.14	48643.280	22.57	0.18
48649,244	22.94	0.29	48649.244	22.53	0.27
48062.920	22.75	0.23	48662.920	22.75	0.23
49000.085	22.59	0.15	48987.302	22.62	0.28
			49000.085	22.56	0.11
C15	P = 11.2		C17	P = 12.7	
48630.549	23.41	0.37	48643.280	21.02	0.09
48643.280	24.05	1.01	48662.920	20.71	0.17
48649.244	23.66	0,38	49000.085	20.95	0.08
48662.920	23.28	0.23			
48987.302	23.28	0.35			
49000.085	23.10	0.27			
C18	P = 36.7		C19	P = 23.6	
48630.549	21.50	0.10	48630.549	22.20	0.17
48643.280	21.72	0.15	48643.280	23.05	0.26
48649.244	21.52	0.12	48649.244	22.97	0.30
48662.920	21.43	0.07	48662.920	22.00	0.22
4S987.302	21.35	0.11	48987.302	22.11	0.21
49000.085	21.44	0.06	49000.085	22.85	0.12
C20	P = 17.0		C21	P = 14.2	
48630.549	22.81	0.18	48630.549	23.07	0.40
4s643.280	22.74	0.16	48643.280	22.34	0.16
48649.244	22.71	0.17	48649.244	21.36	0.64
48662.920	22.81	0,20	48662.920	22.74	0.13
48987.302	23.34	0.52	48987.302	22.71	0.2?2
49000,0s5	22.15	0.24	49000.085	22.42	0.34

Table 5- Continued

JD + 2400000	I	σ_I	JD + 2400000	I	σ_I
C22	P = 13.6		C23	1' = 11.7	
48630.549	22.08	0.17	48630.549	22.90	0.28
48643.280	22.02	0.08	48643.280	22.79	0.36
48649.244	22.37	0.20	48649.244	22.$)0	0.28
48662.920	22.30	0.14	48662.920	23.24	0.34
48987.302	22.20	0.16	49000.085	22.77	0.13
49000,0ss	22.24	0.11			
C26	P = 54.8		C28	P = 27.6	
48630.815	20.57	0.11	48630.815	21.94	0.21
48643.153	20.39	0.14	48643.153	21.44	0.17
48649.113	20.60	0.11	48649.113	21.52	0.18
48663.120	20.71	0.12	48663.120	22.36	0.16
48987.441	20.70	0.14	48987.441	21.73	0.20
49000.291	21.06	0.15	49000.291	21.40	0.16
C29	P = 30.0		C30	P = 18.1	
48630.815	21.32	0.15	48630.815	21.84	0.23
48643.153	21.62	0.16	48643.153	22.71	0.29
48649.113	21.14	0.12	48649.113	21.92	0.21
4s663.12?0	21.35	0.15	48663.120	22.33	0.19
48987.441	21.19	0.15	48987.441	22.23	0.21
49000.291	21.52	0,10	49000.291	22.07	0.23

Table 6: Properties of M81 Eclipsing Variable

ID	x	y	P (days)	$< V >$	$< I >$	N_{sig}
Major Axis Chip 1						
E1	623.8	63.7	21.1	22.64	22.57	1,7

Table 7: Error Budget For The True Distance Modulus To M81

Error	Source of Error
± 0.10	Errors in ALLFRAME photometry; PSF uncertainty
± 0.03	Extinction and transformation errors
± 0.05	Calibration of ALLFRAME zero point
± 0.06	Error in mean of M81 PL relation ($= \sigma/\sqrt{N-1}$)
± 0.10	Uncertainty in LMC + M81 absorption
± 0.05	Error in mean of the LMC PL relation ($= \sigma/\sqrt{N-1}$)
± 0.10	Uncertainty in LMC true distance modulus
± 0.07	Uncertainty due to metallicity
± 0.20	Error in M81 true modulus

"1'able 8: Comparison of Distances to M81

Method	Distance Modulus μ_o	Distance Mpc	Reference
Brightest Stars, HII	27.70 ± 0.3	3.47	de Vaucouleurs (1 978)
IR Tully-Fisher	27.86 ± 0.3	3.73	Aaronson, Mould, & Huchra (1 980)
B-Band Cepheids	28.73	5.57	Sandage (1984)
B-Band Tully-Fisher	27.60+ 0.16	3.31	Bottinelli *et al.* (1984)
I-Band Cepheids	27.59 ± 0.31	3.30	Freedman & Madore (1988)
Planetary Nebula Luminosity Function	27.72 ± 0.25	3.50	Jacoby *et al.* (1989)
Surface Brightness Fluctuations	27.72 ± 0.18	3.50	Tonry (1991)
Cepheids Observed with the HST	27.80 ± 0.20	3.63	This Paper

Note: Sandage (1984) value corrected for Galactic foreground reddening of $A_B = 0.07$ mag given in that paper.

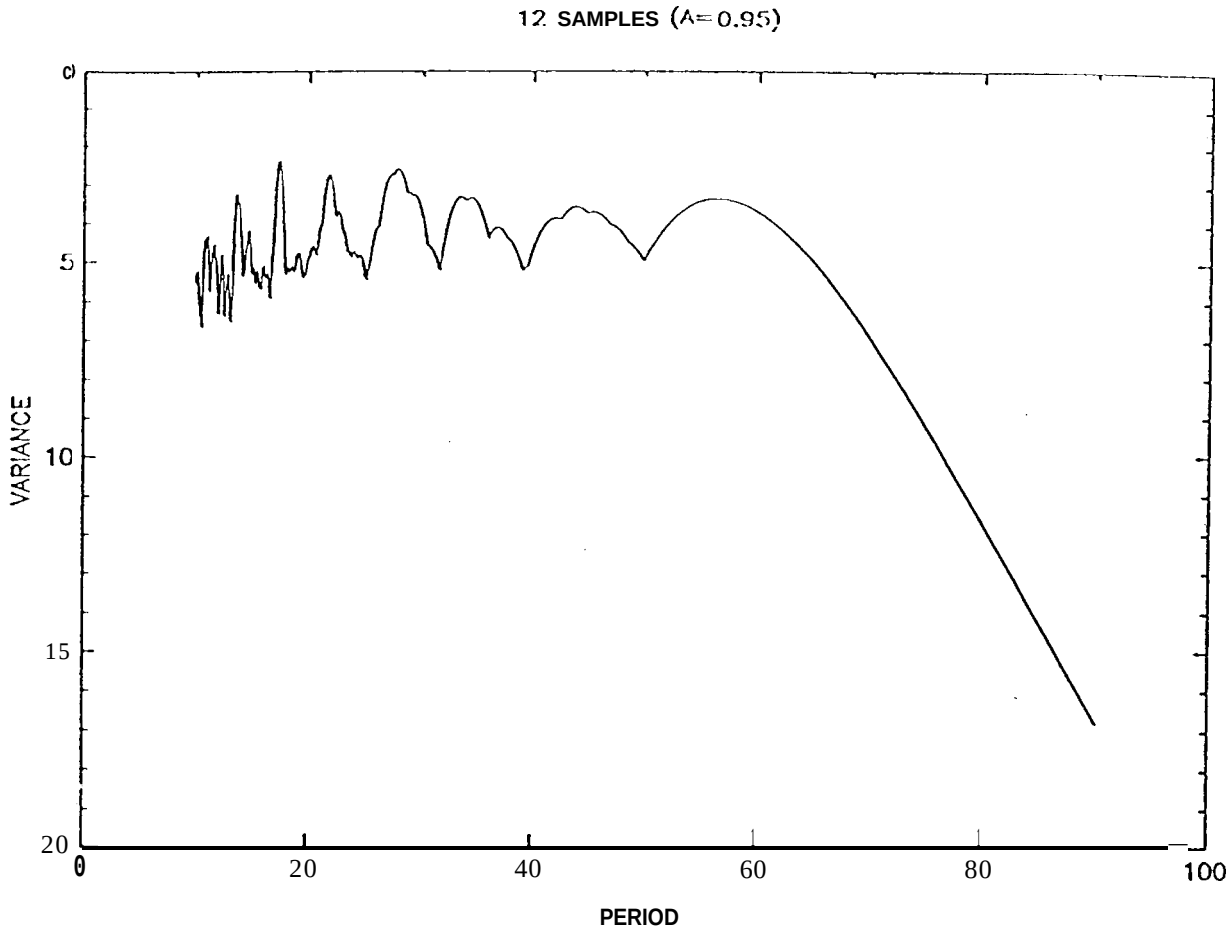

Figure la

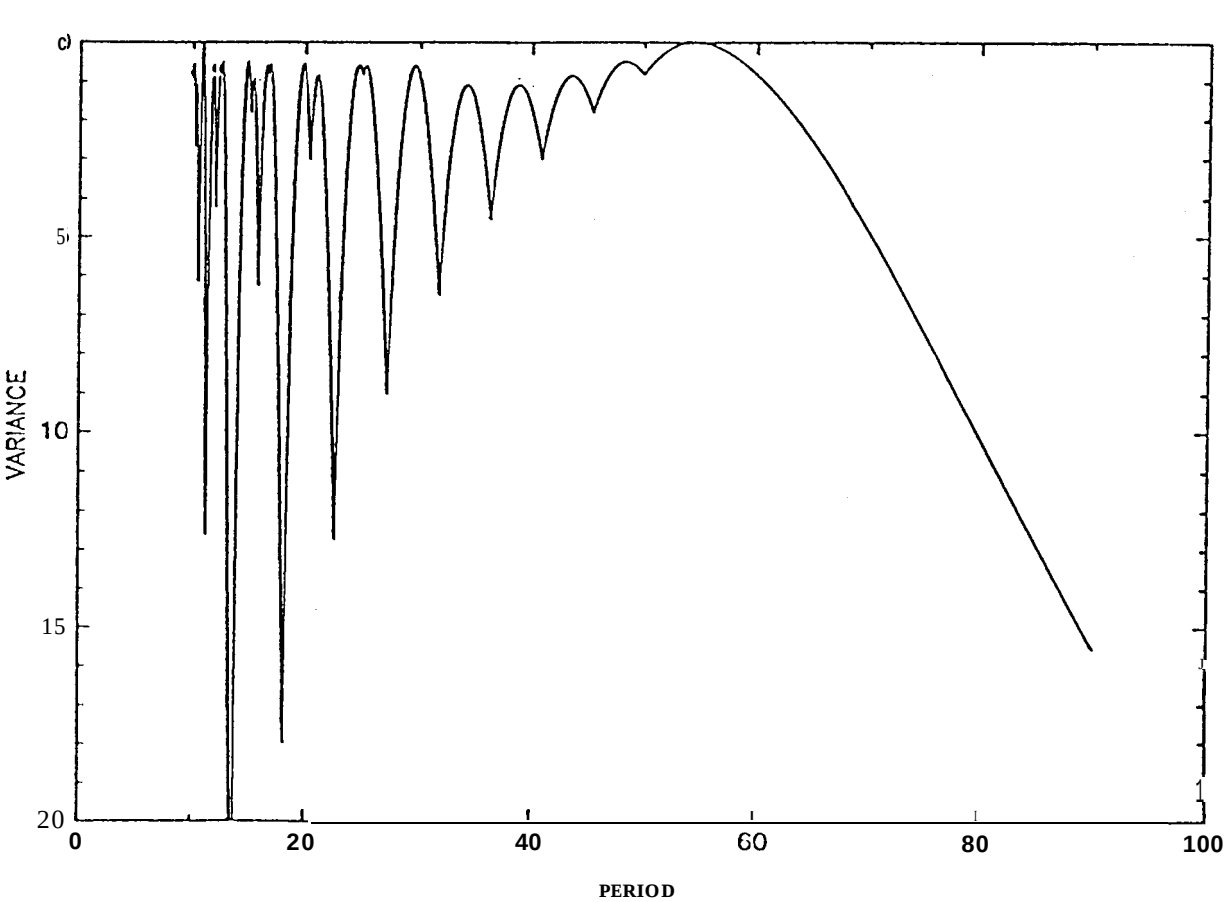

Figure 1b

Figure 1

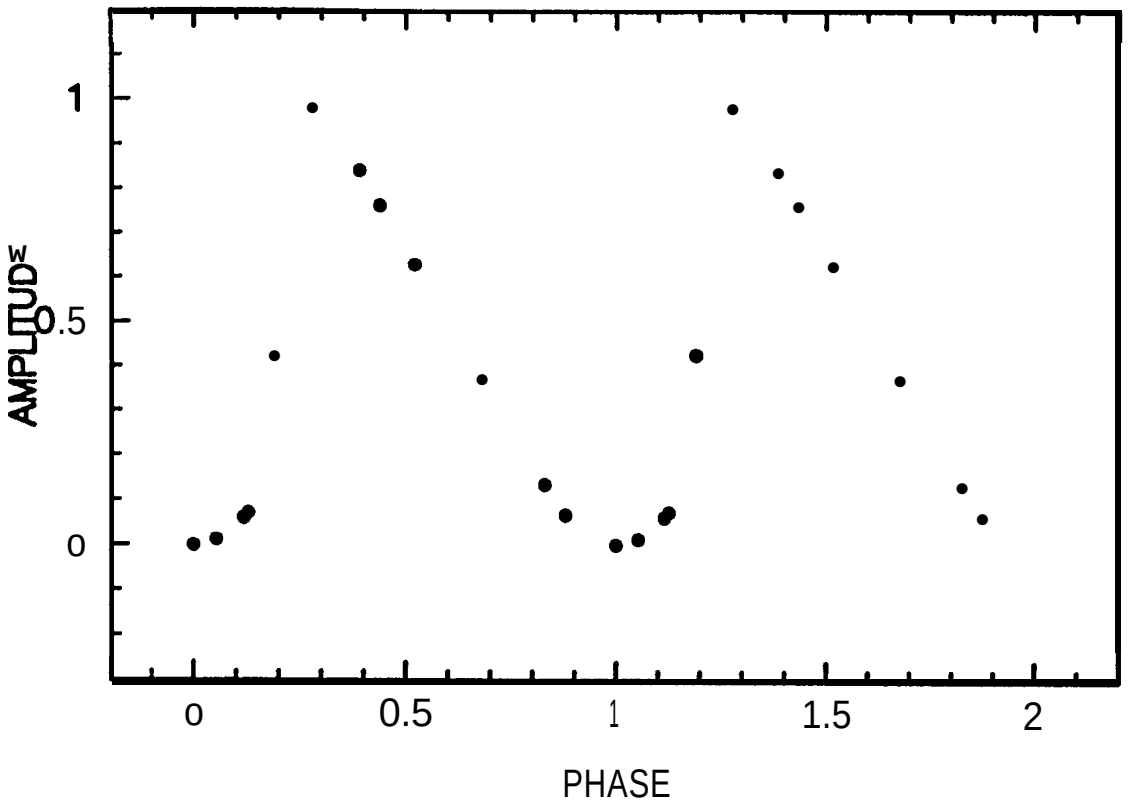

Figure 2a

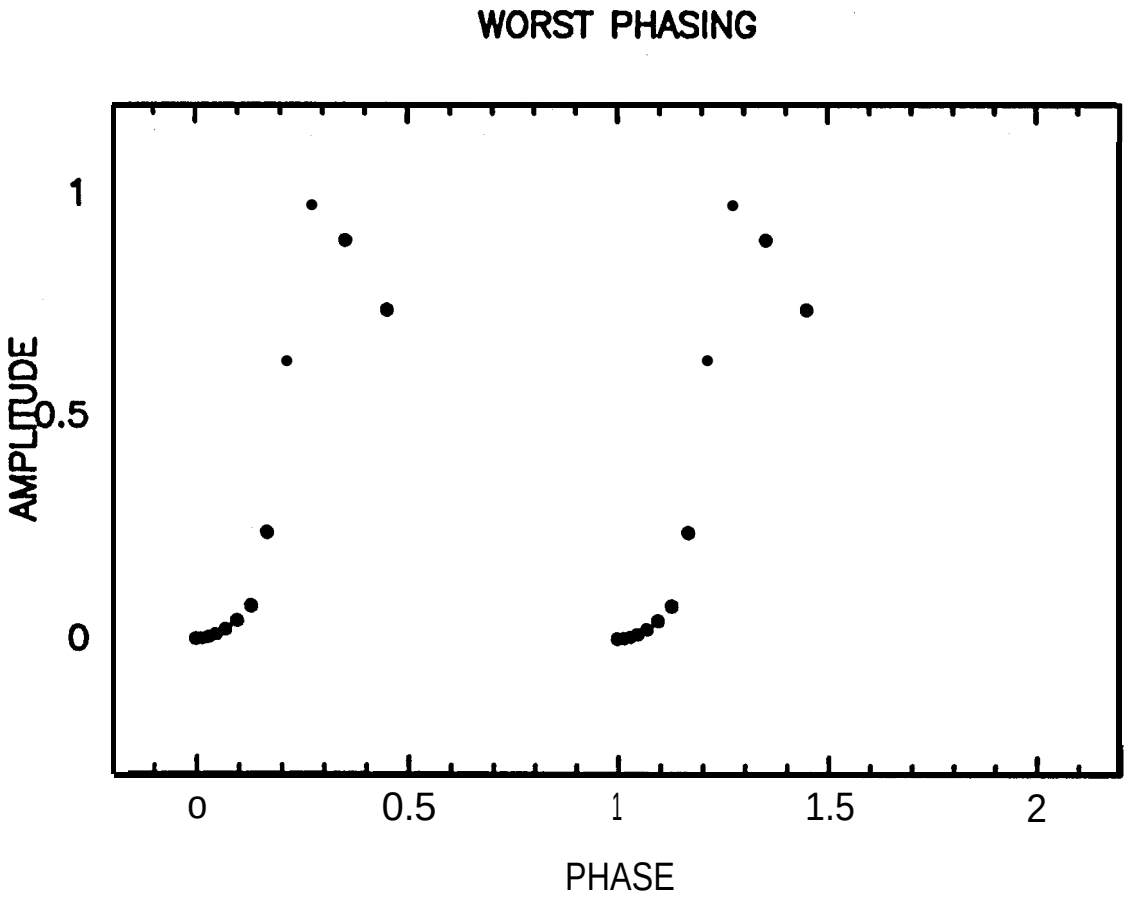

Figure 2b

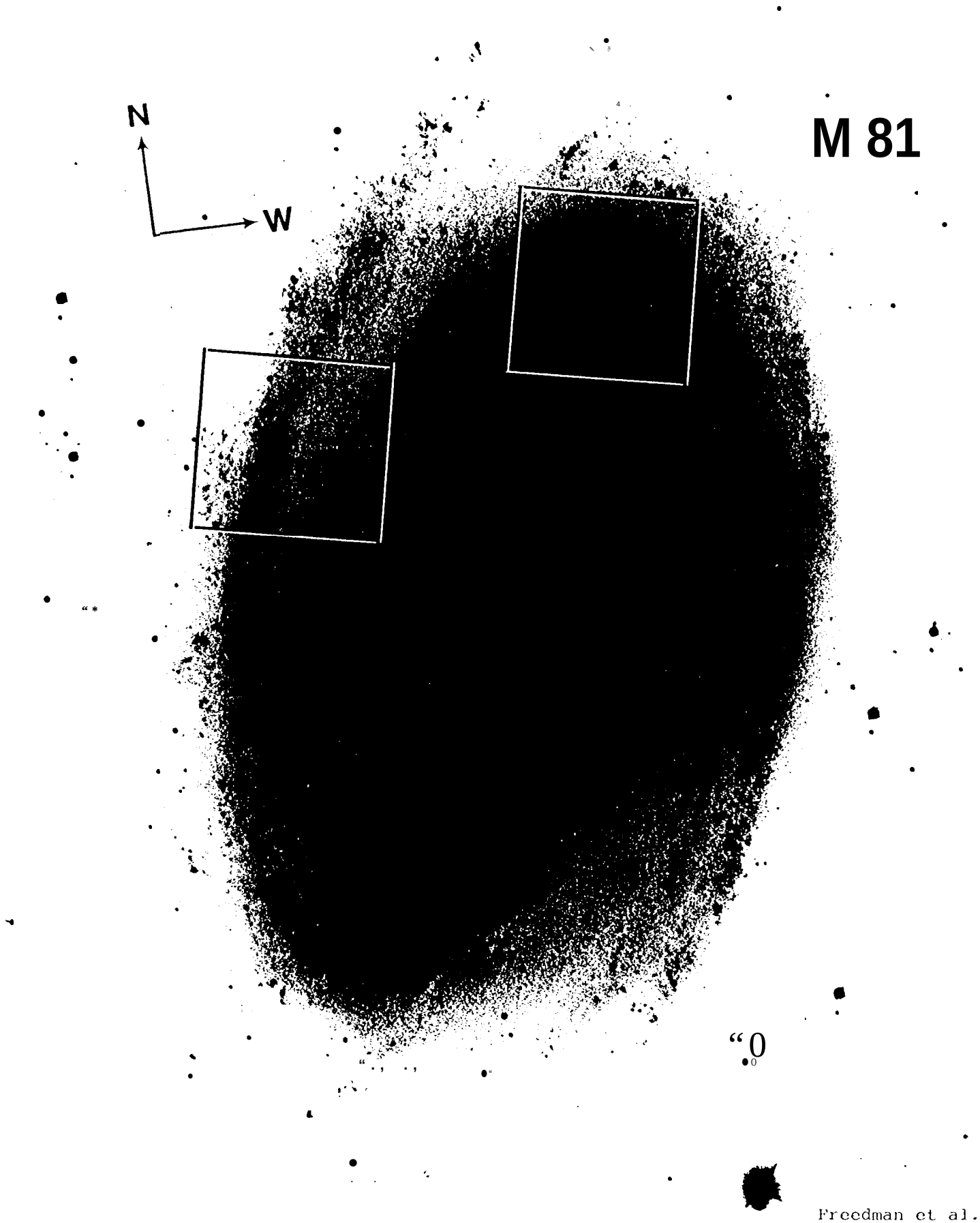

Freedman et al.
Figure 3

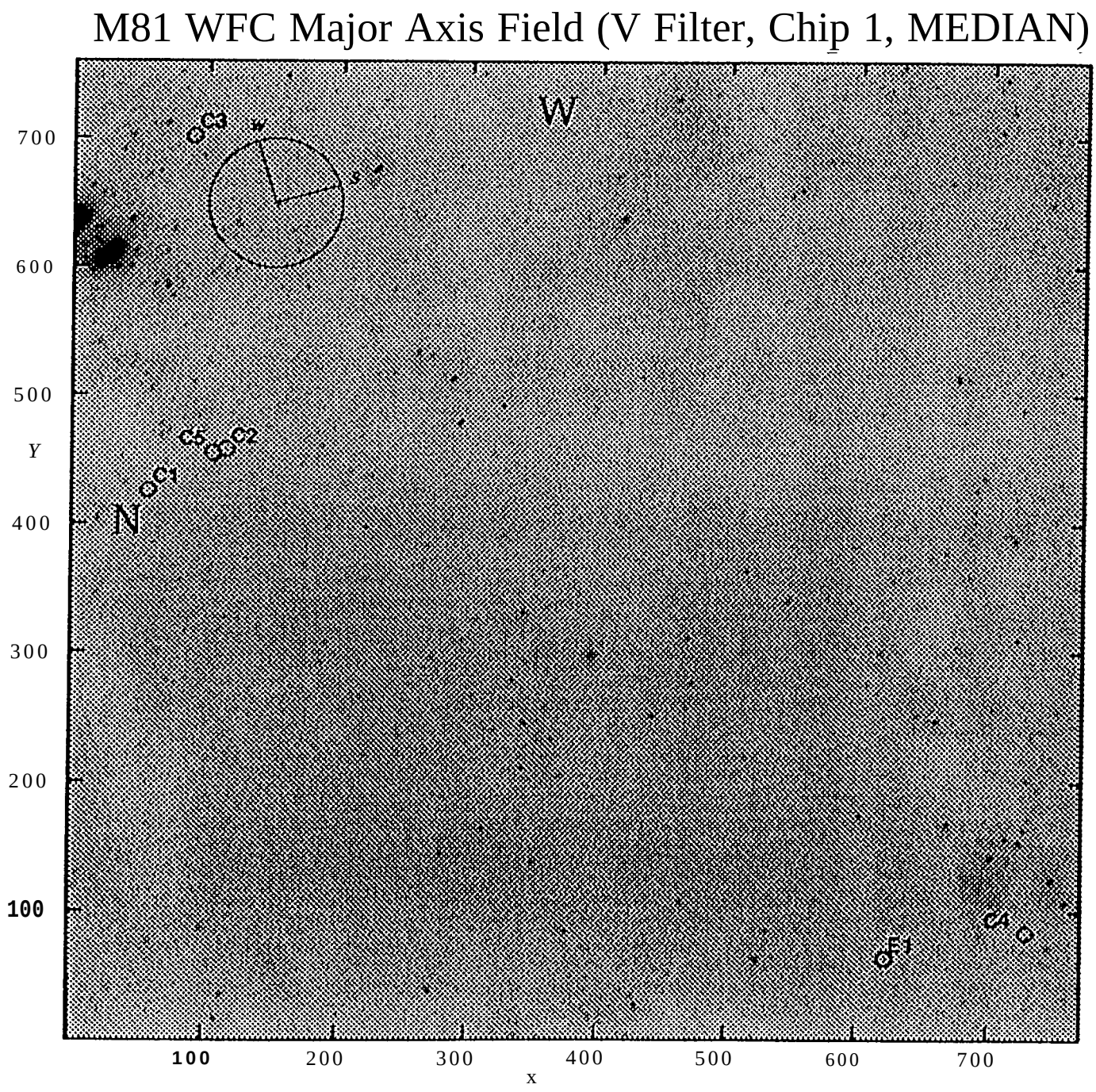
M81 WFC Major Axis Field (V Filter, Chip 1, MEDIAN)
W
N
C1
C2
C3
C4
C5
F1
700
600
500
400
300
200
100
Y
100
200
300
400
500
600
700
X

Figure 4a

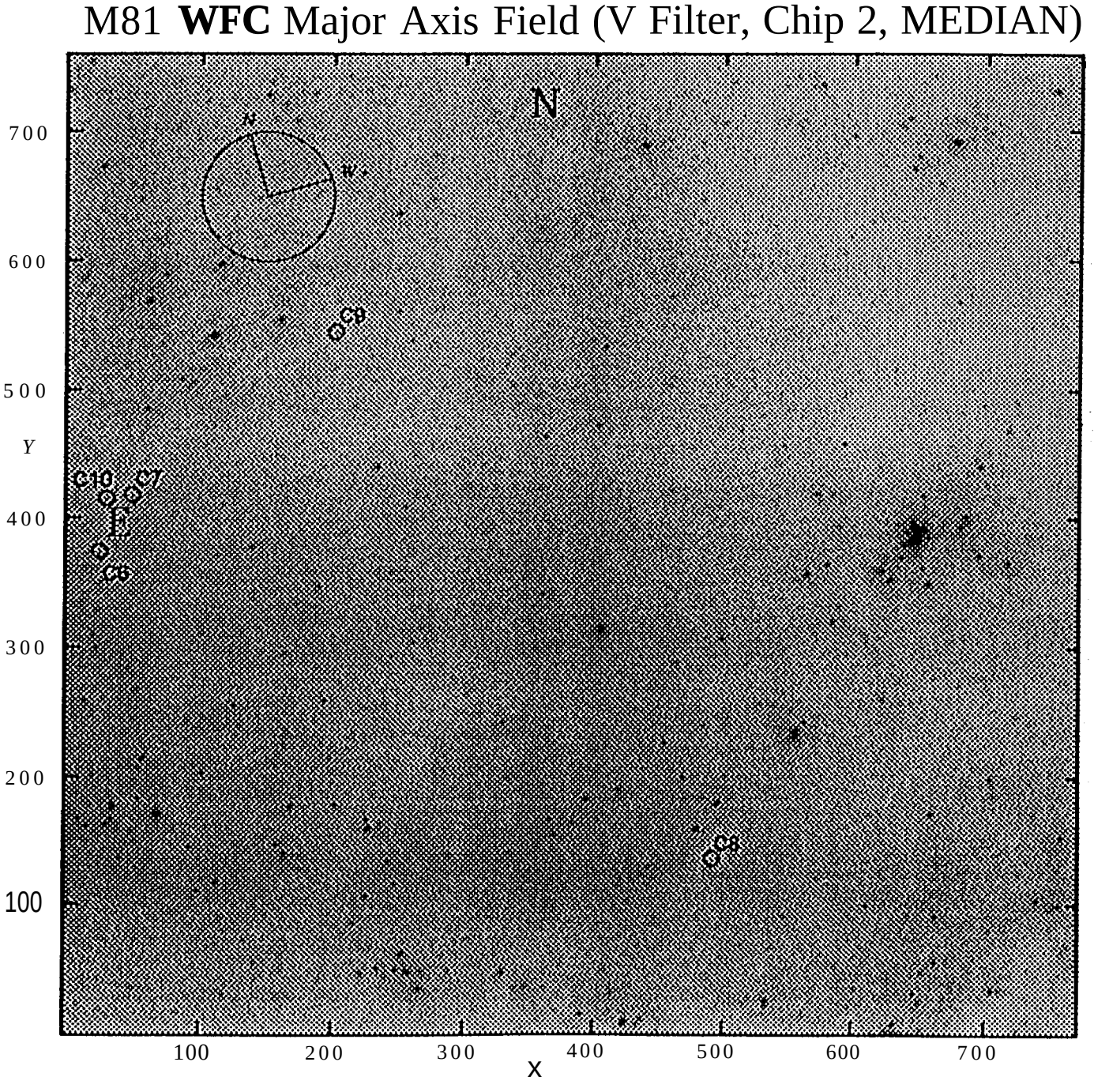
M81 WFC Major Axis Field (V Filter, Chip 2, MEDIAN)
N
E
C9
C10
C7
C6
C3
700
600
500
400
300
200
100
Y
100
200
300
400
500
600
700
X

Figure 4b

M81 WFC Major Axis Field (V Filter, Chip 3, MEDIAN)

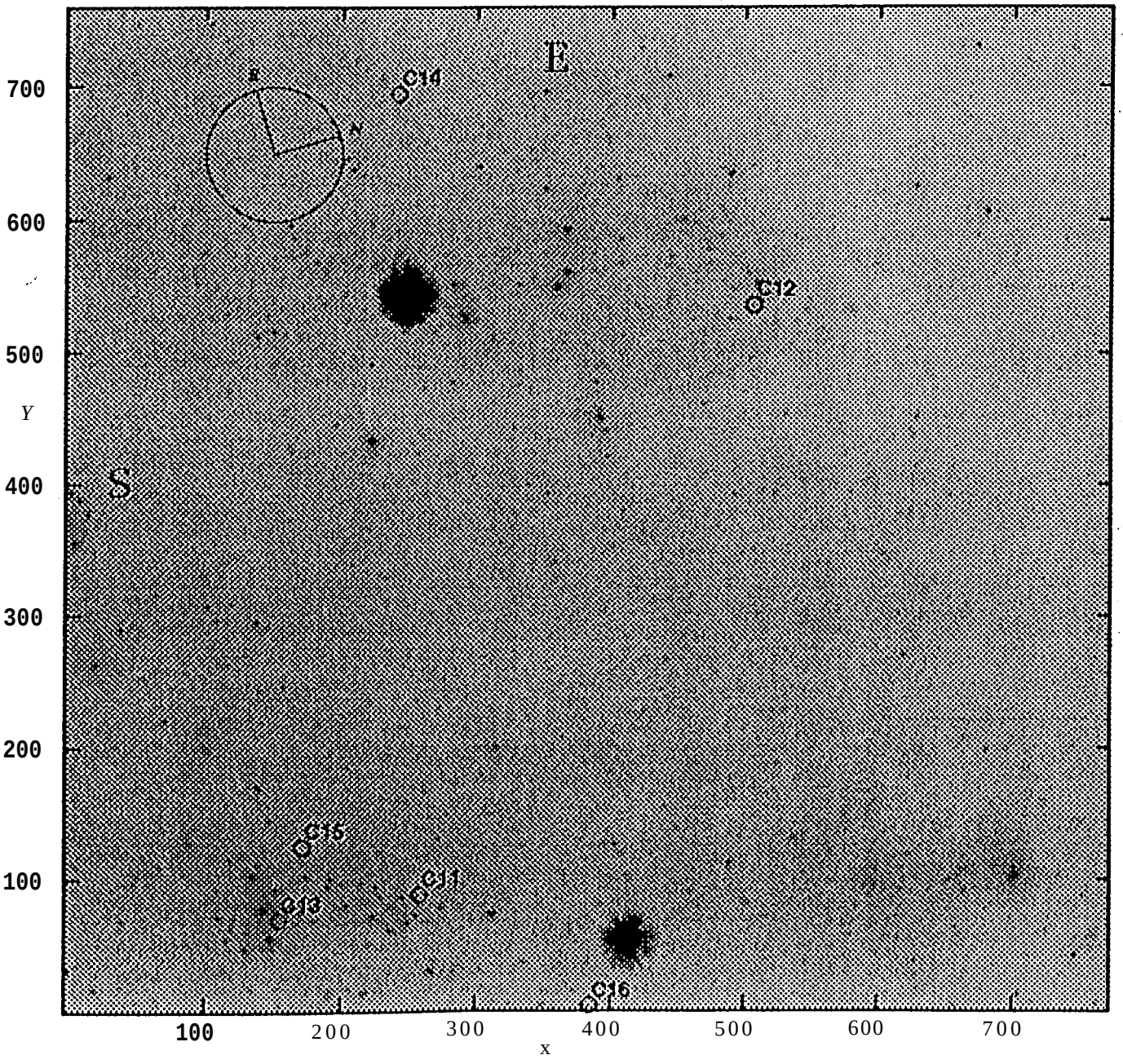

Figure 4c

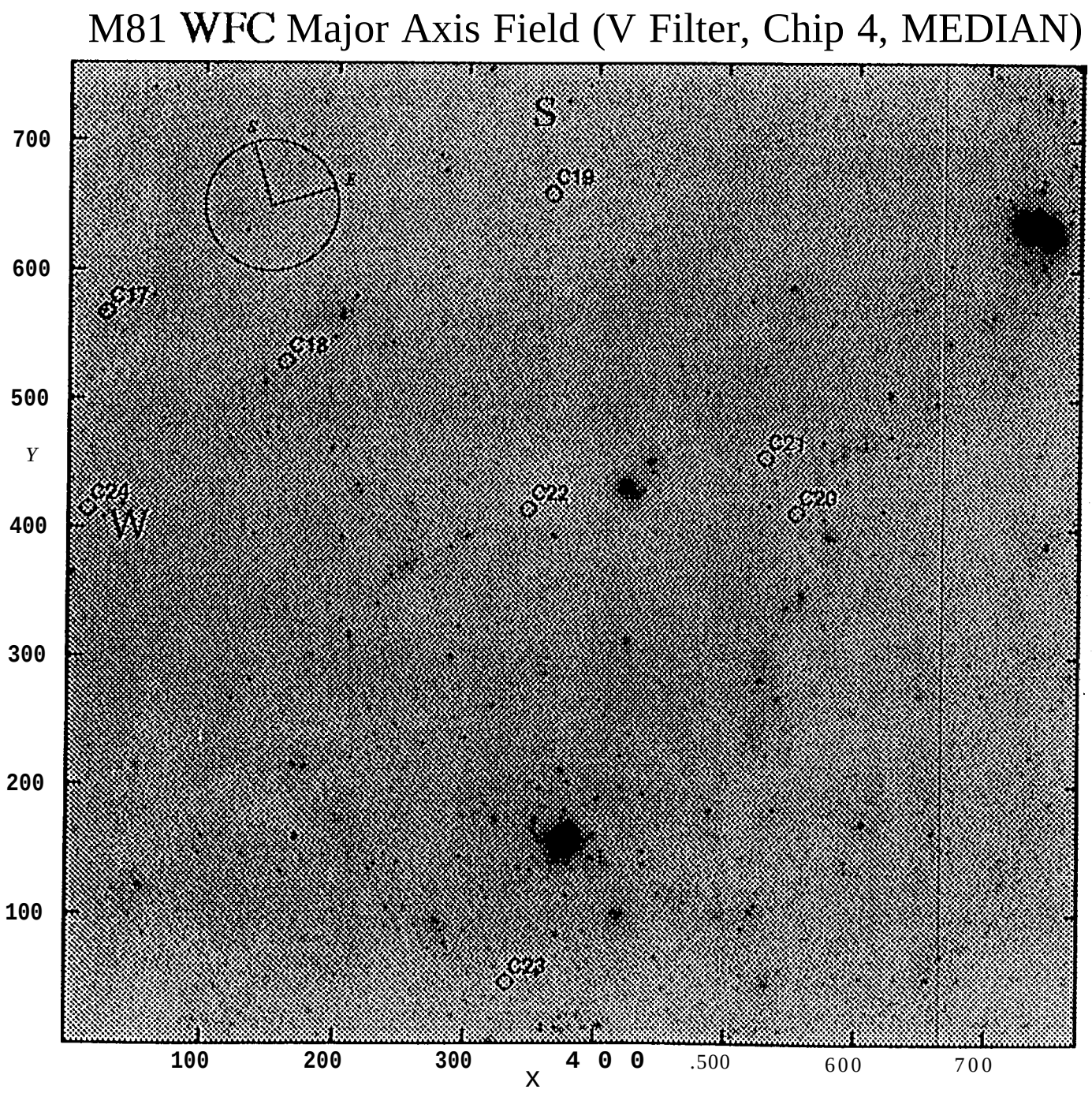
M81 WFC Major Axis Field (V Filter, Chip 4, MEDIAN)
S
C19
C17
C18
C21
C22
C20
C24
W
C23
700
600
500
Y
400
300
200
100
100
200
300
4 0 0
.500
600
700
X

Figure 4d

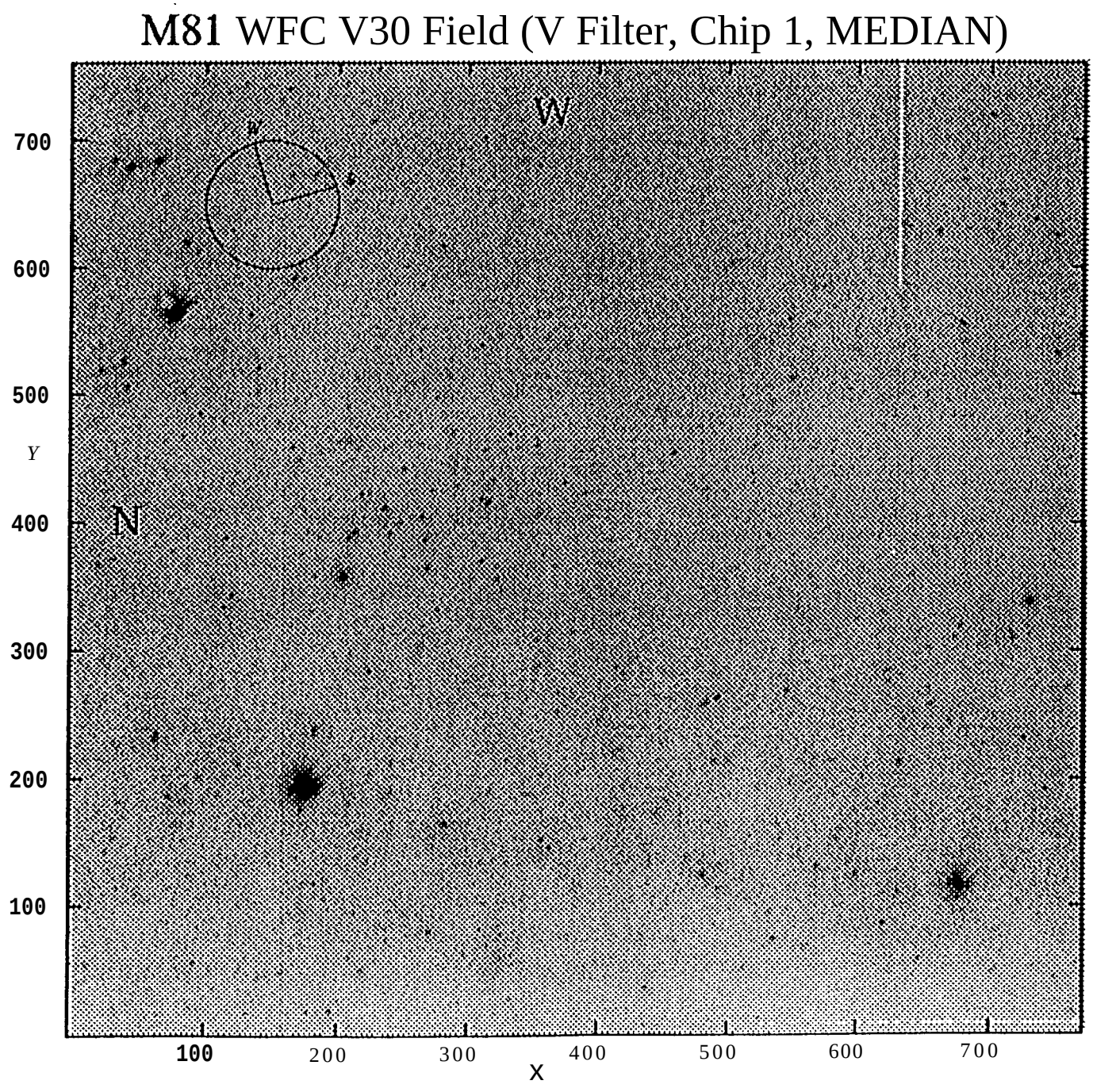
M81 WFC V30 Field (V Filter, Chip 1, MEDIAN)
W
N
N
700
600
500
Y
400
300
200
100
100
200
300
400
500
600
700
X

Figure 5a

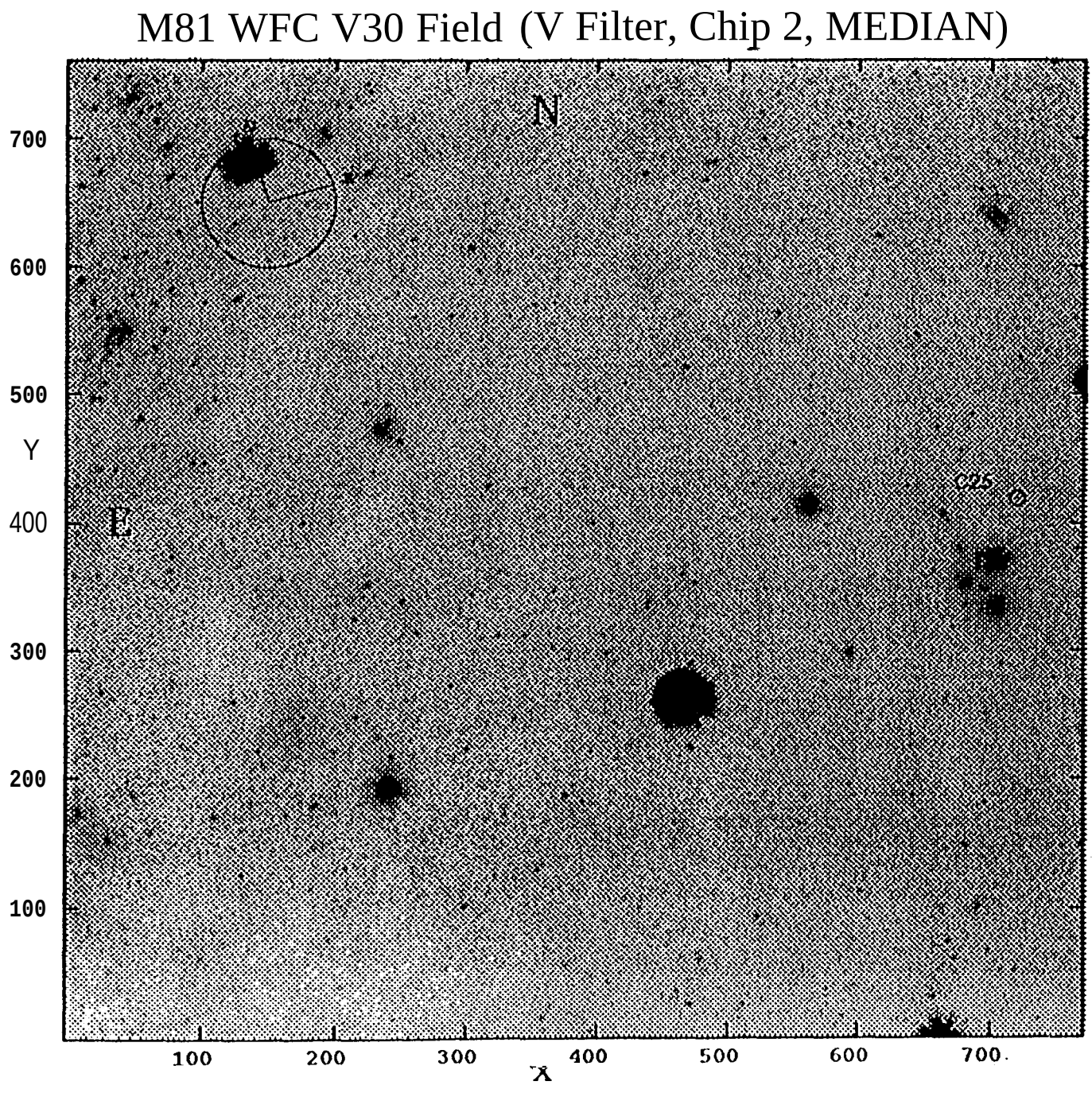
M81 WFC V30 Field (V Filter, Chip 2, MEDIAN)
N
E
C25
700
600
500
Y
400
300
200
100
100
200
300
400
500
600
700
X

Figure 5b

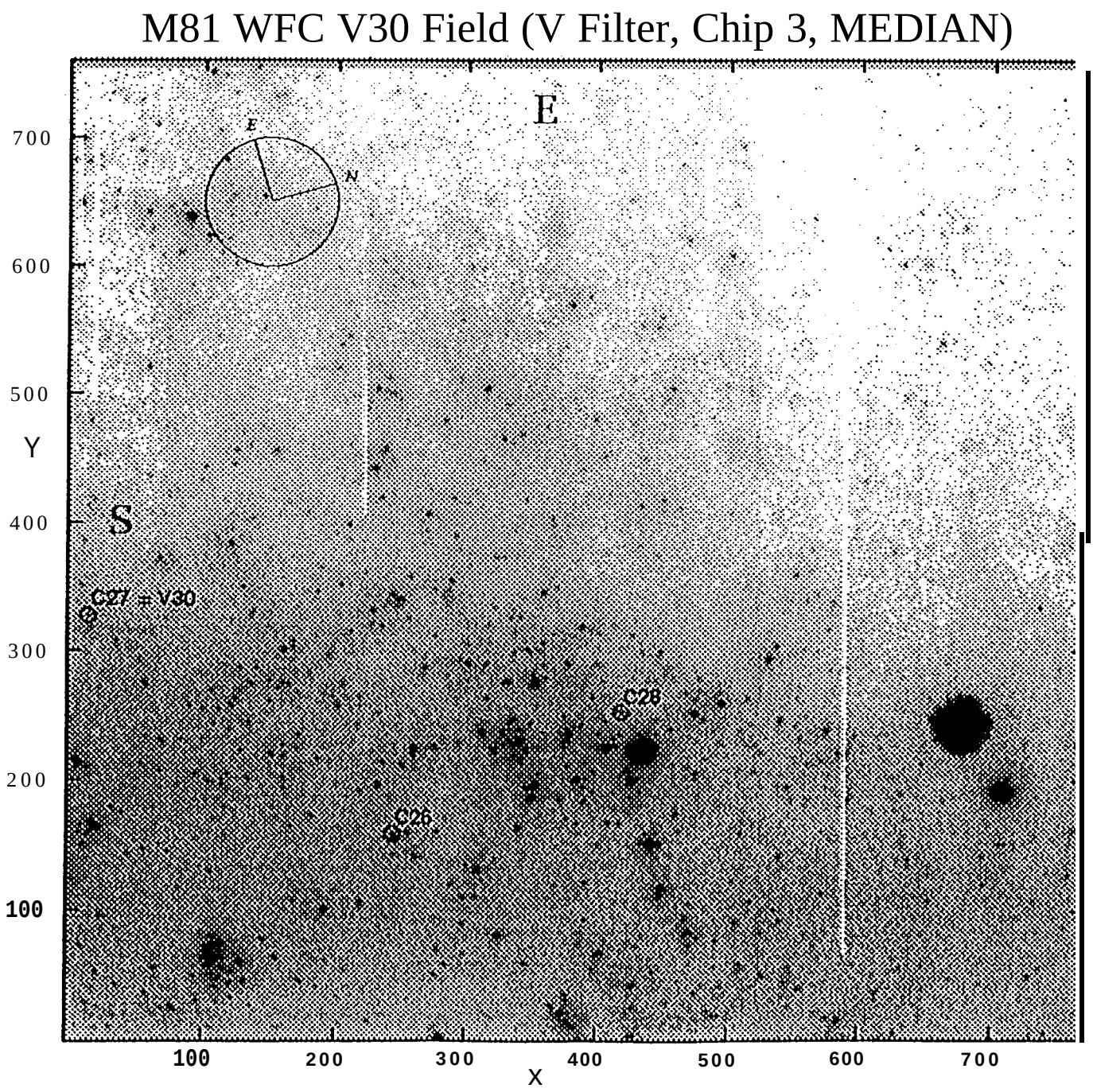
M81 WFC V30 Field (V Filter, Chip 3, MEDIAN)
E
E
N
S
C27 = V30
C28
C26
700
600
500
Y
400
300
200
100
100
200
300
400
500
600
700
X

Figure 5c

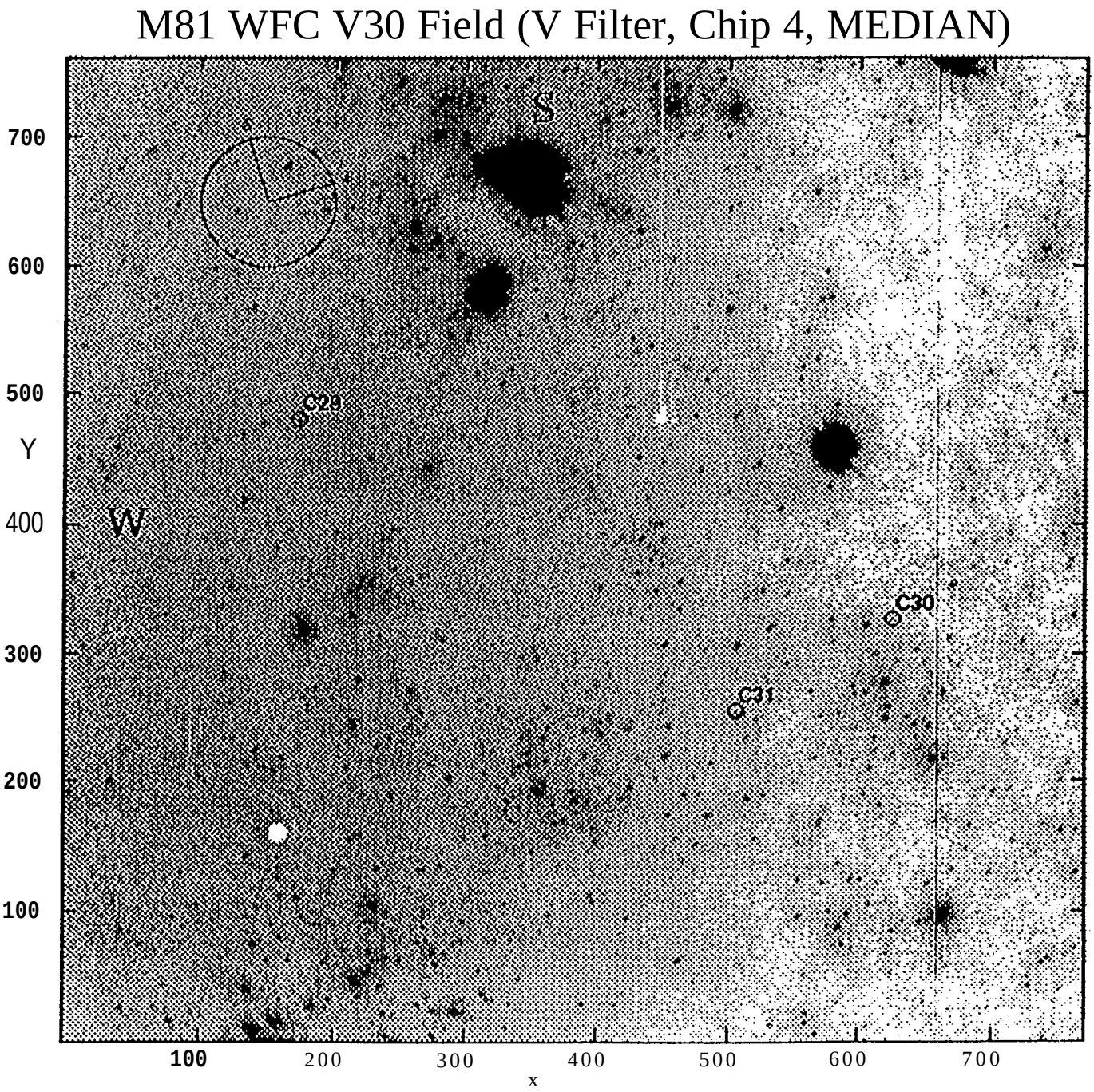
M81 WFC V30 Field (V Filter, Chip 4, MEDIAN)
S
W
C29
C30
C31
700
600
500
Y
400
300
200
100
100
200
300
400
500
600
700
x

Figure 5d

C 1

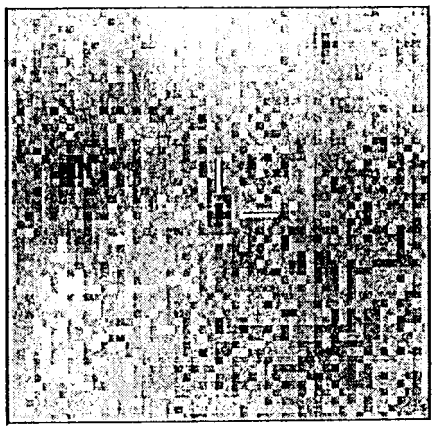

C 2

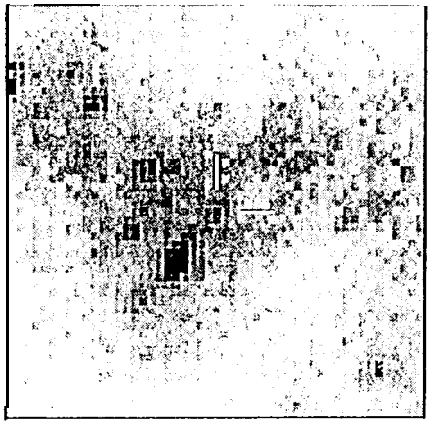

C 3

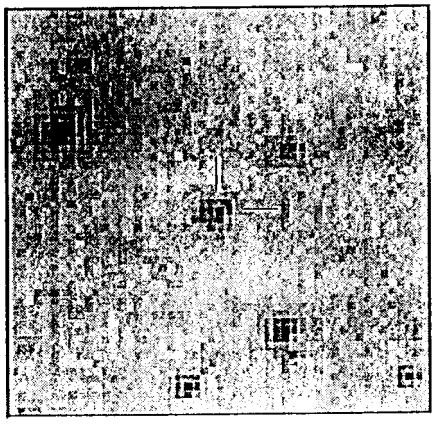

C 4

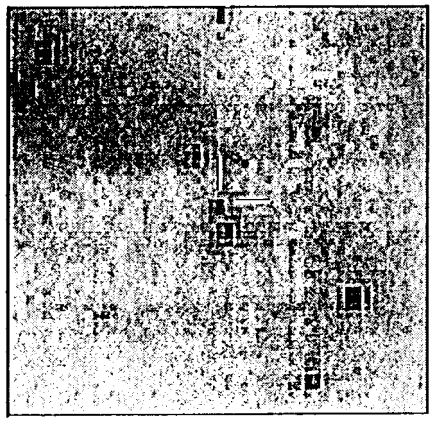

C 5

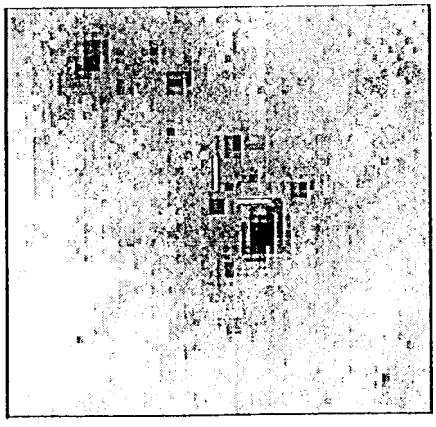

C 6

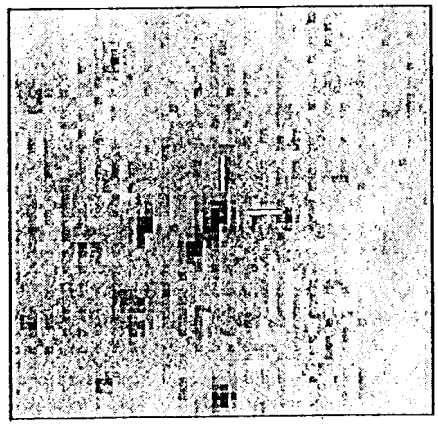

Freedman et al.

Figure 6

c 7

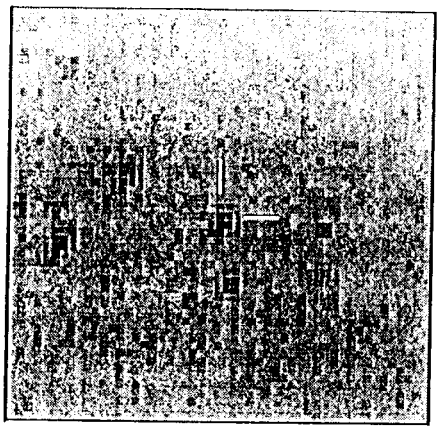

C 8

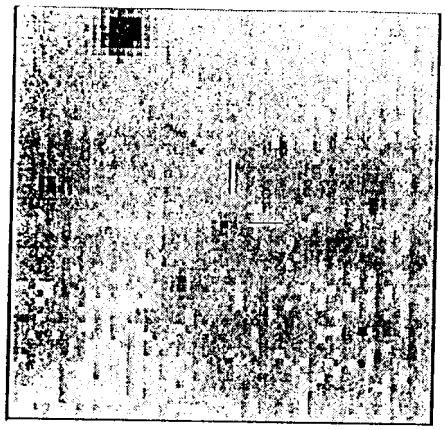

c 9

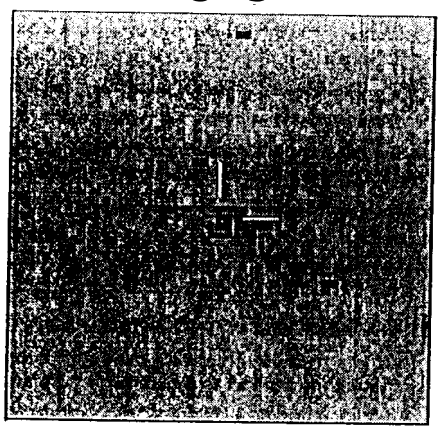

C10

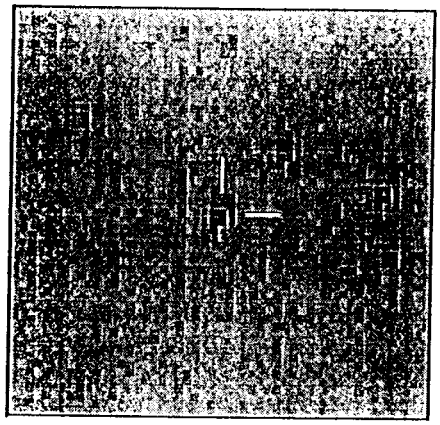

C11

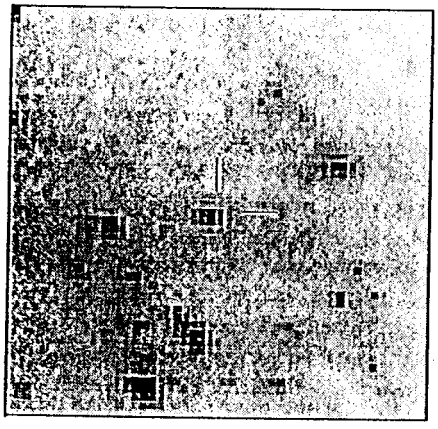

C12

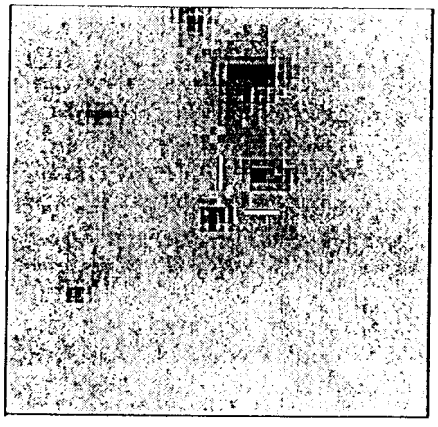

Freedman et al.

Figure 6 con't

C13

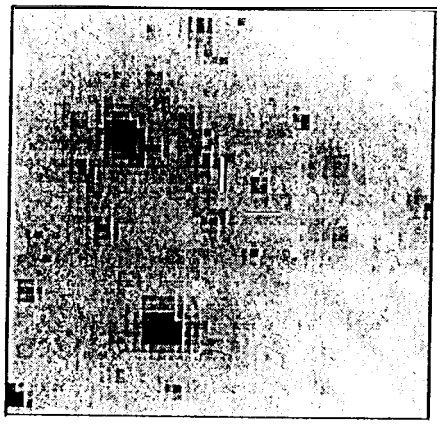

C14

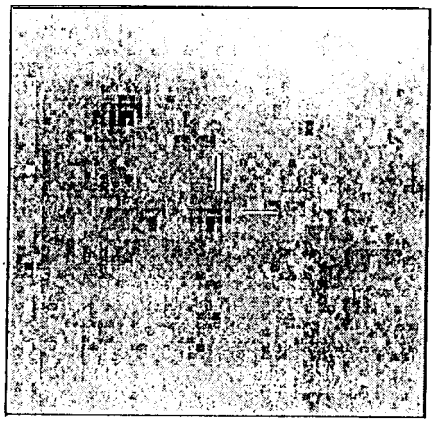

C15

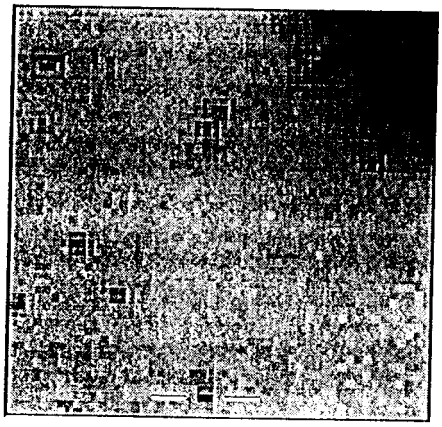

C16

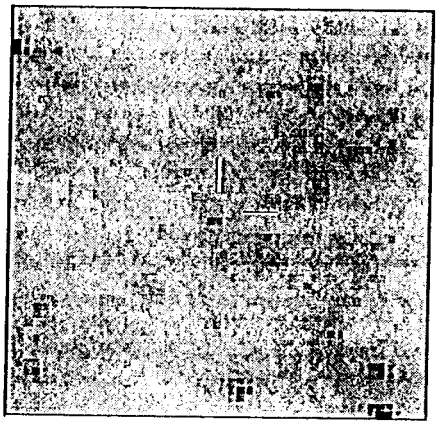

C17

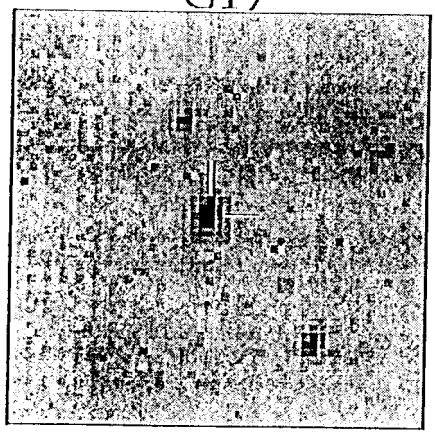

C18

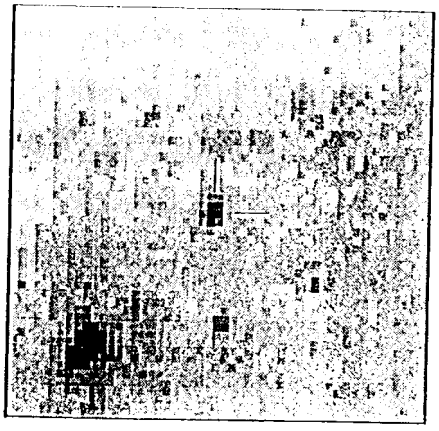

Freedman et al.

Figure 6 con't

(.;:19

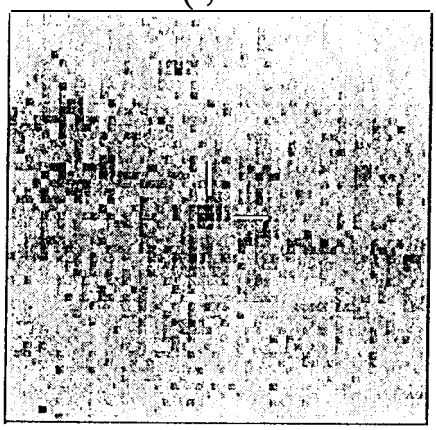

C20

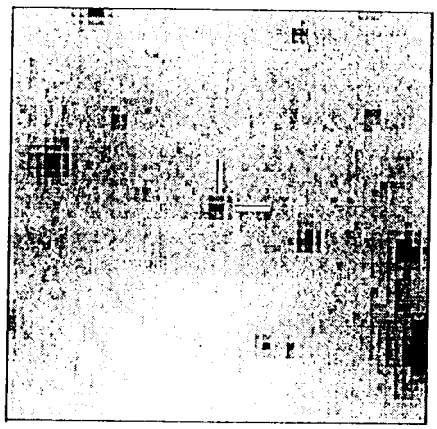

C21

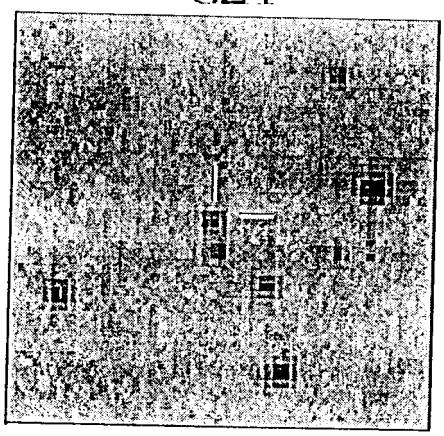

C22

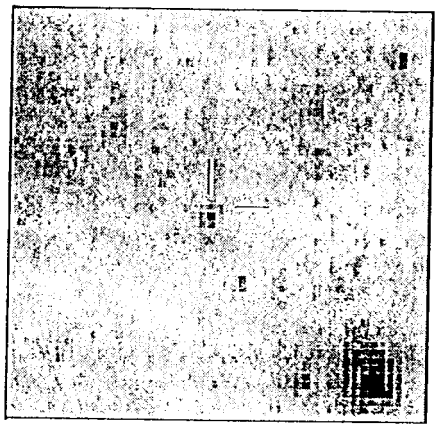

C23

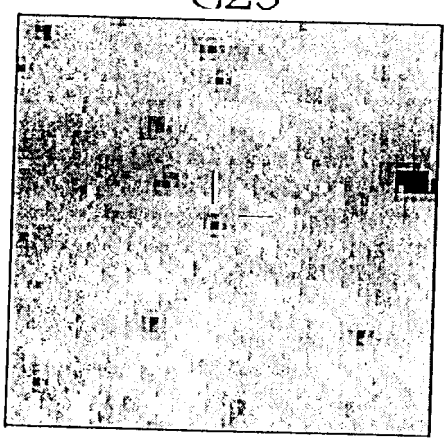

C24

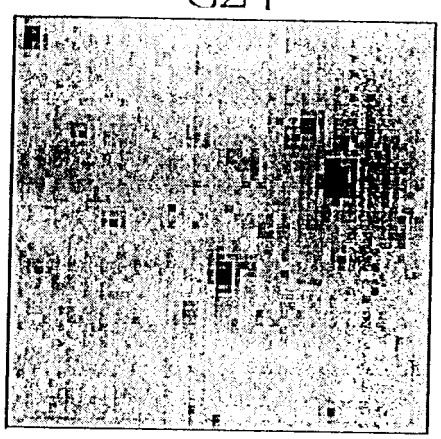

Figure 6 con't

C25

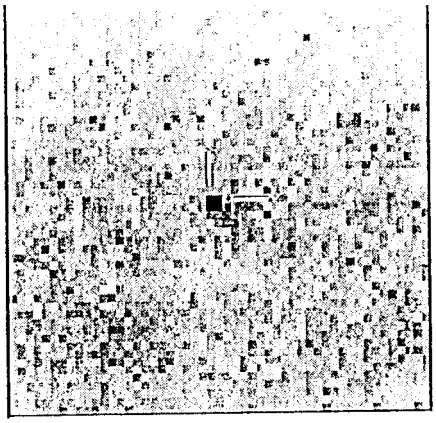

C26

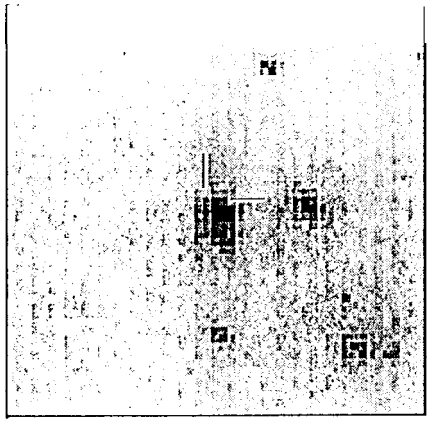

C27

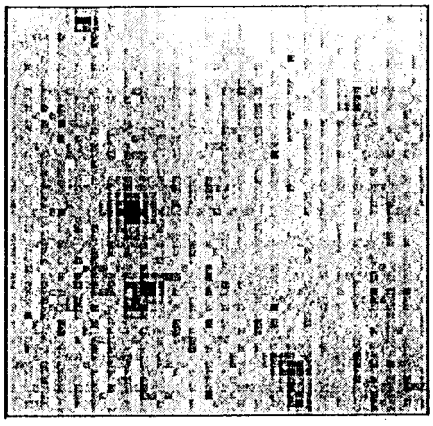

C28

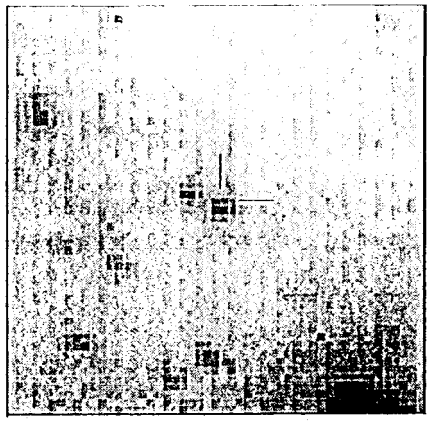

C29

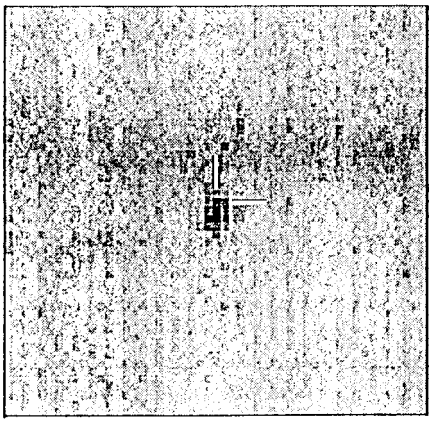

C30

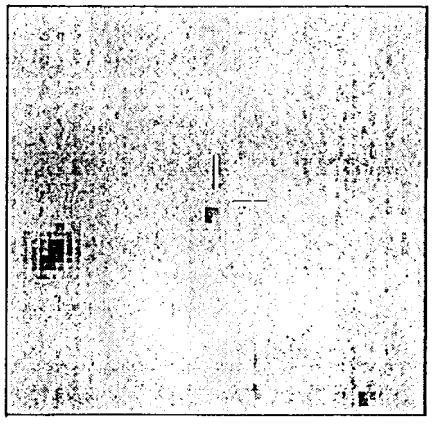

Freedman et al

Figure 6 con't

C31

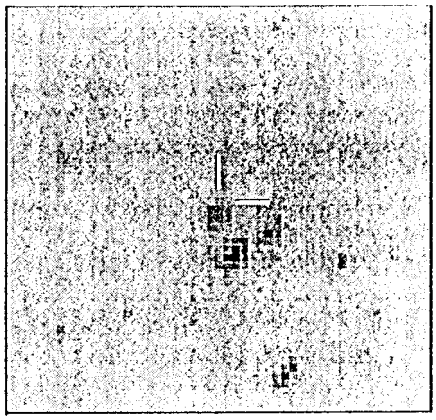

Freedman et al.

Figure 6 con't

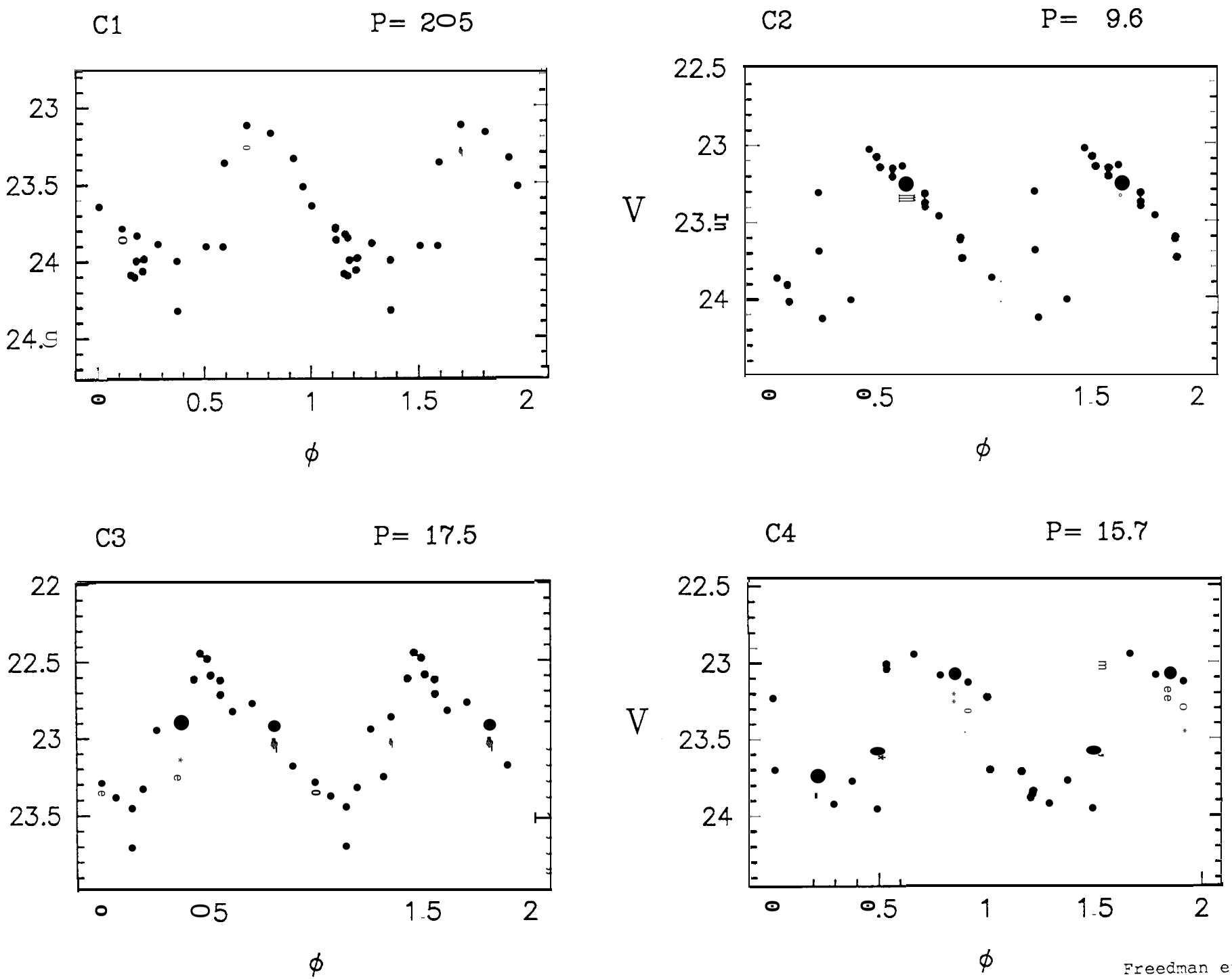

Freedman et al.
Figure 7a

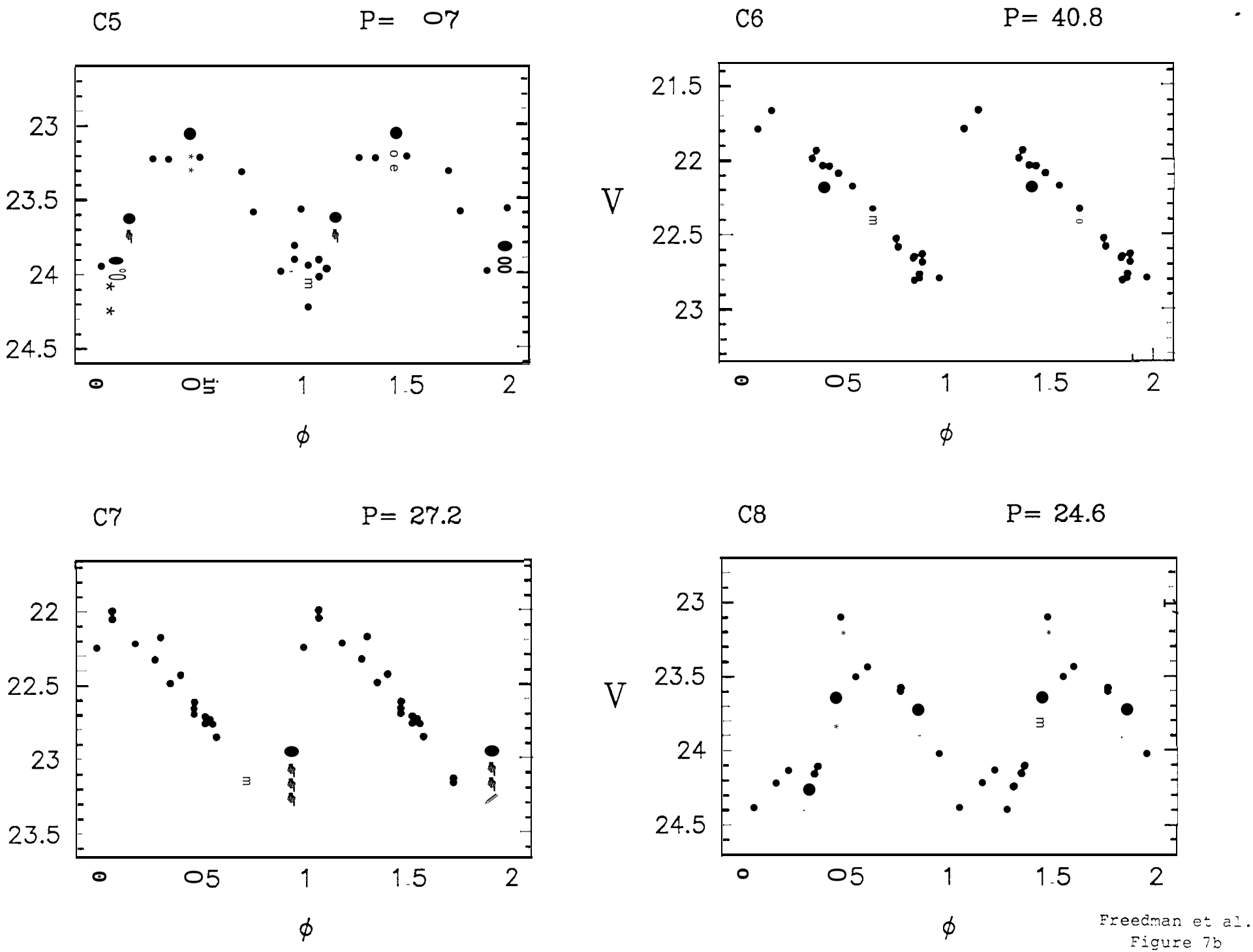

Freedman et al.
Figure 7b

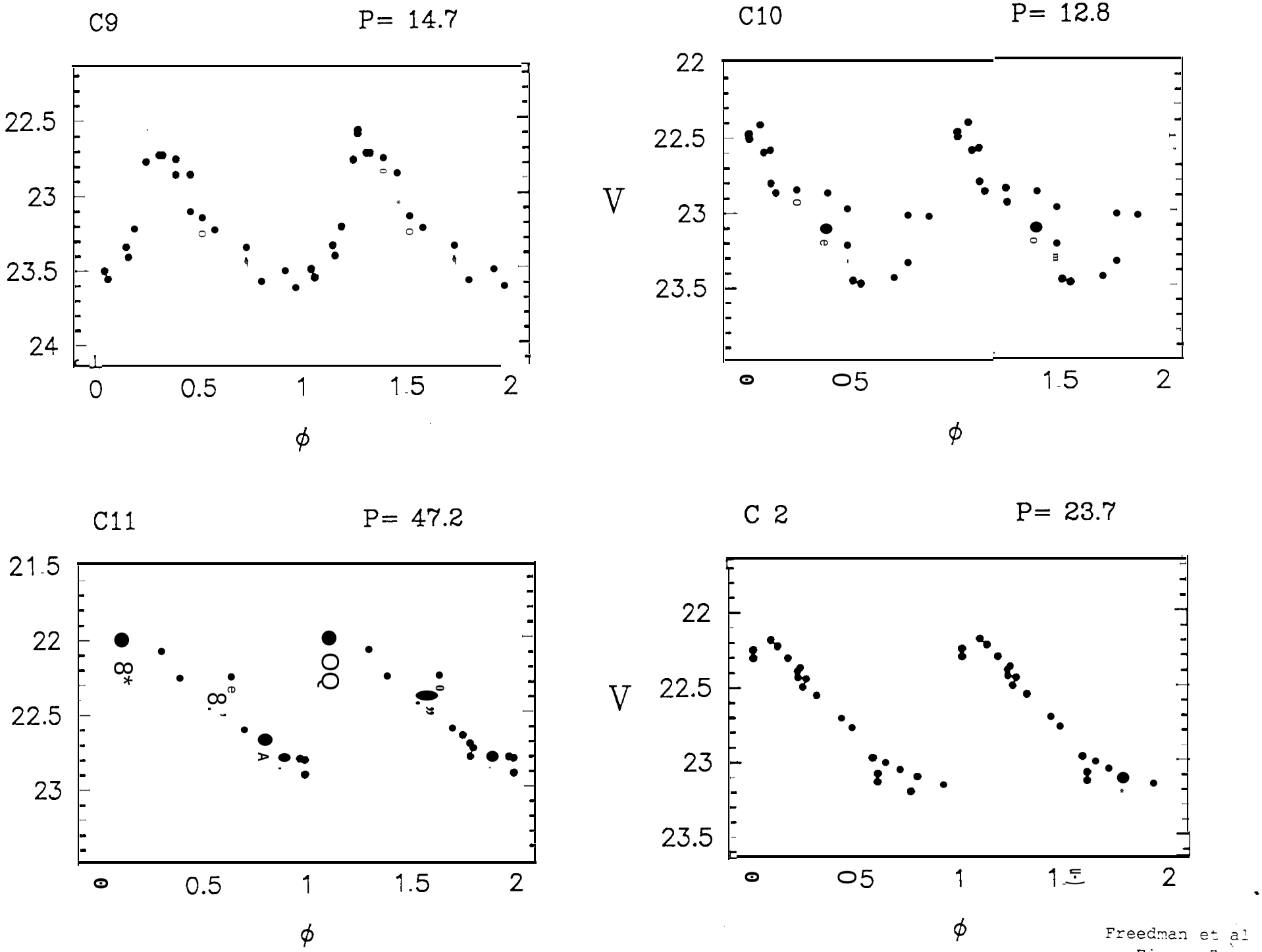

Freedman et al
Figure 7c

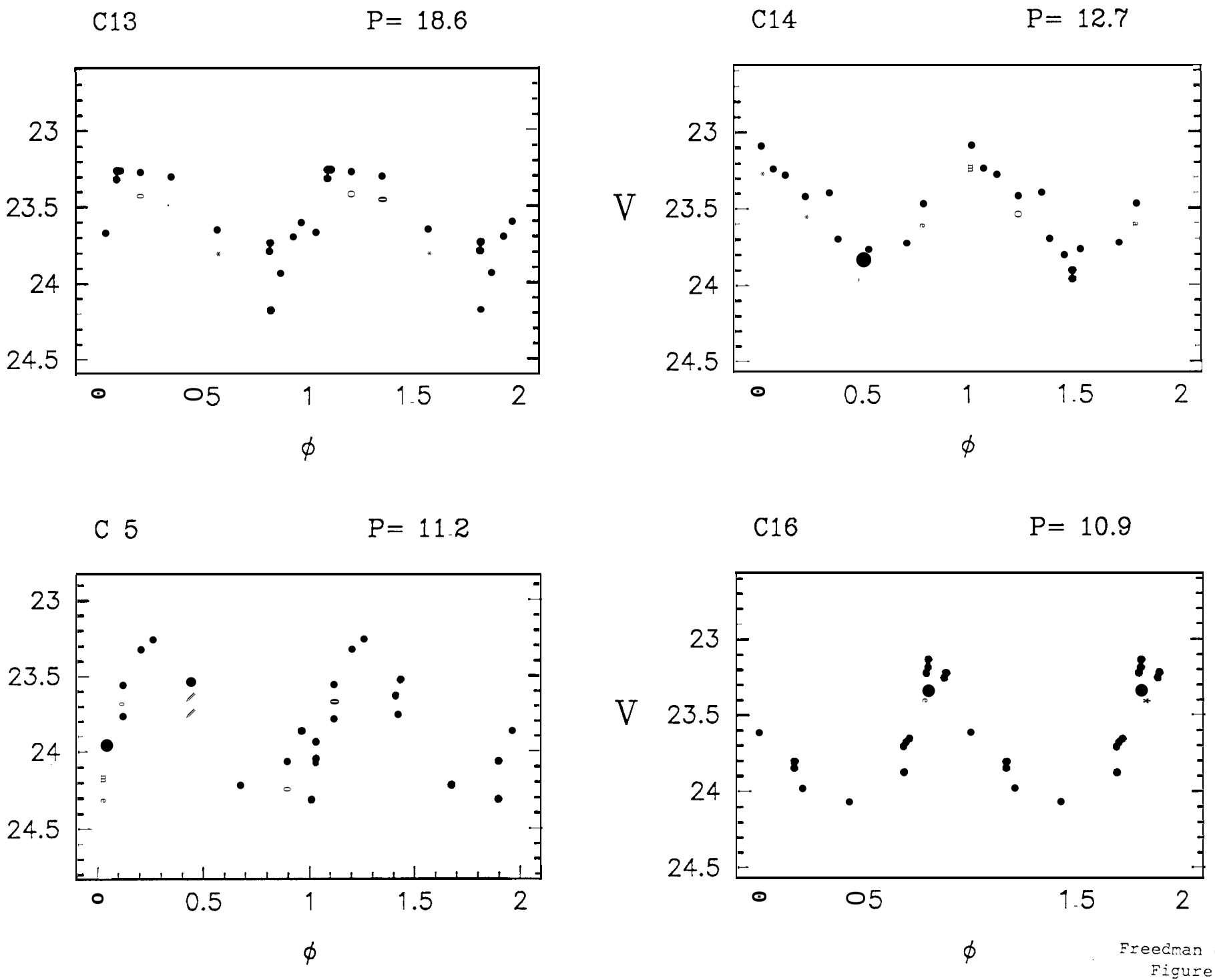

Freedman et al.
Figure 7d

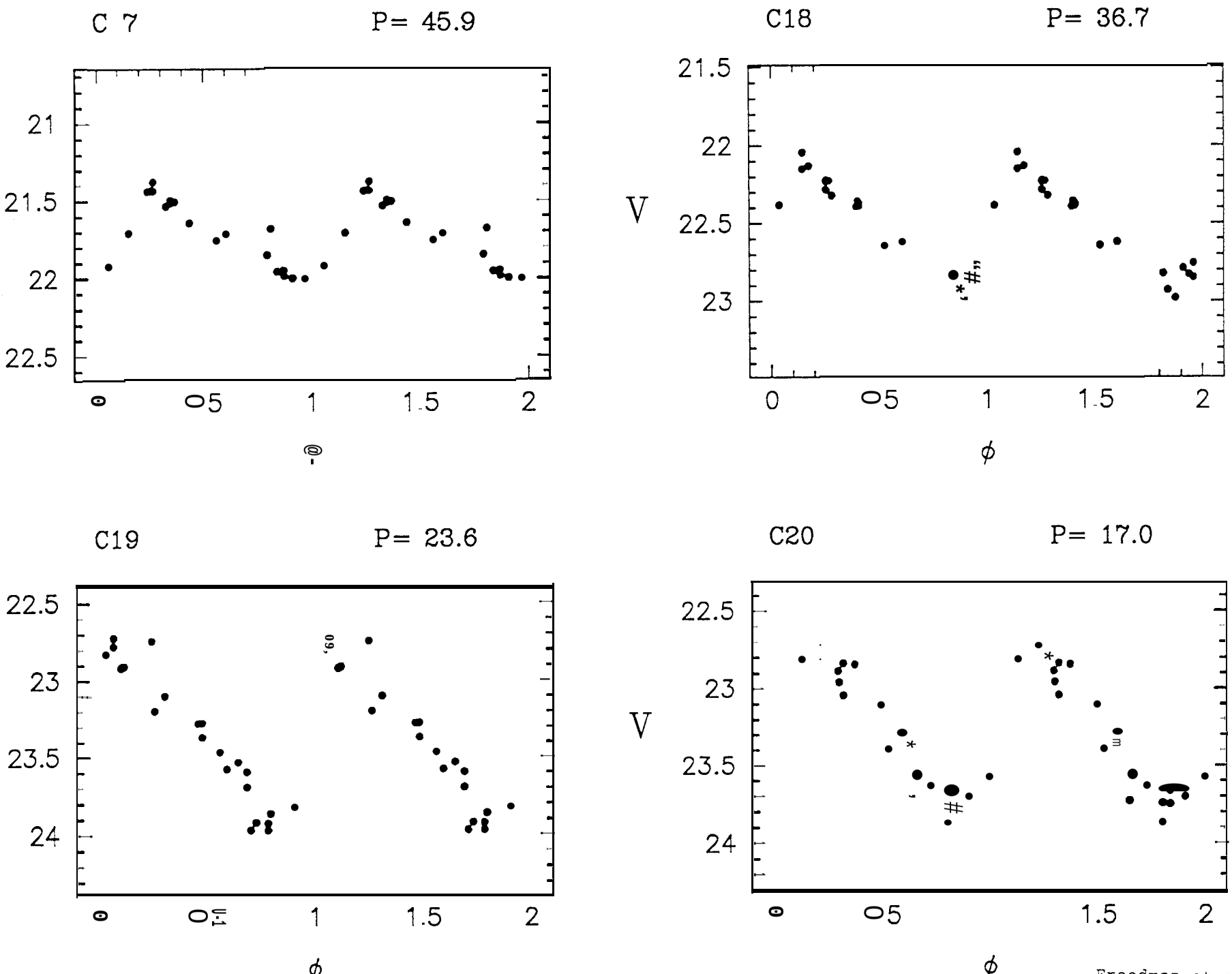

Freedman et al.
Figure 7e

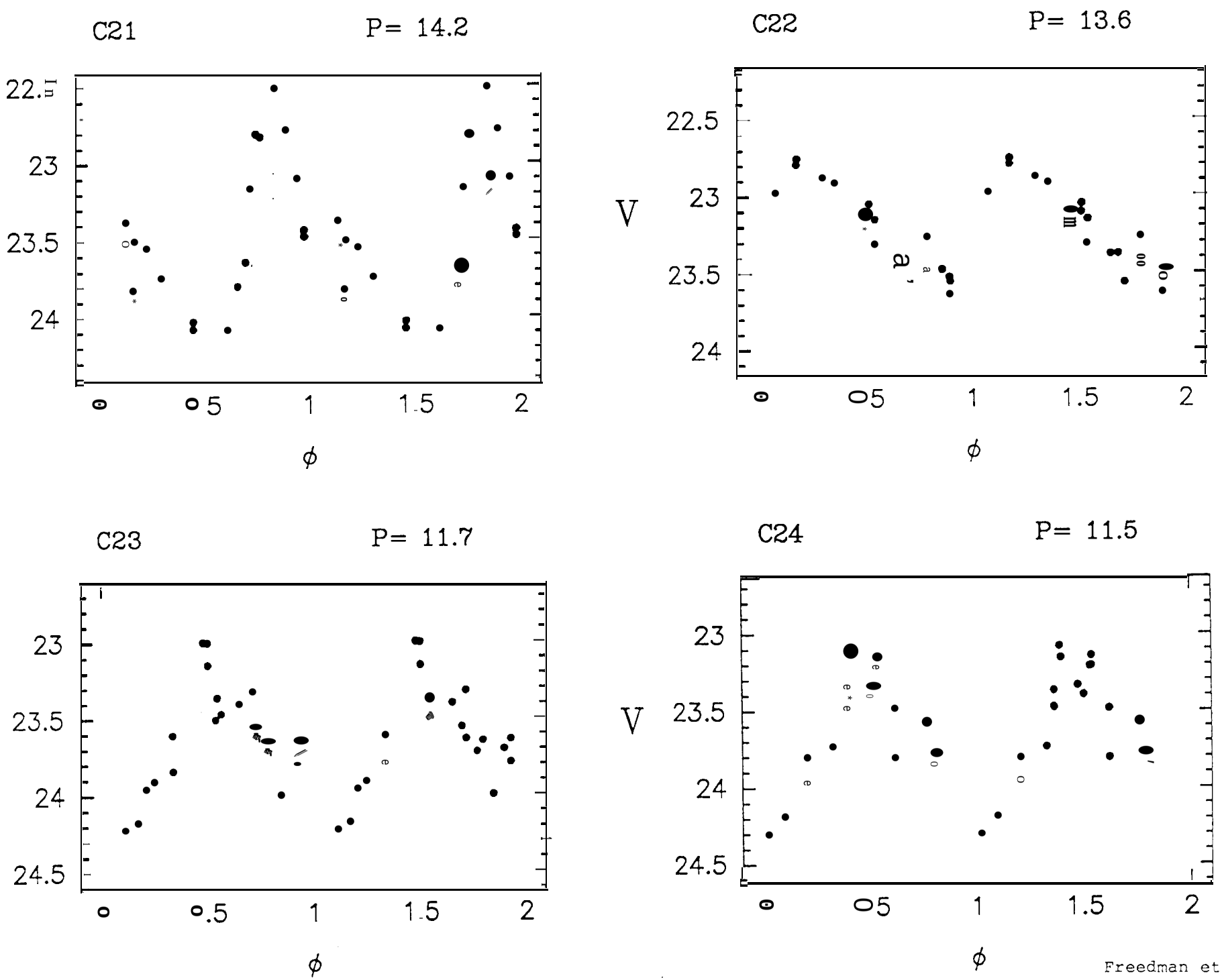

Freedman et al.
Figure 7f

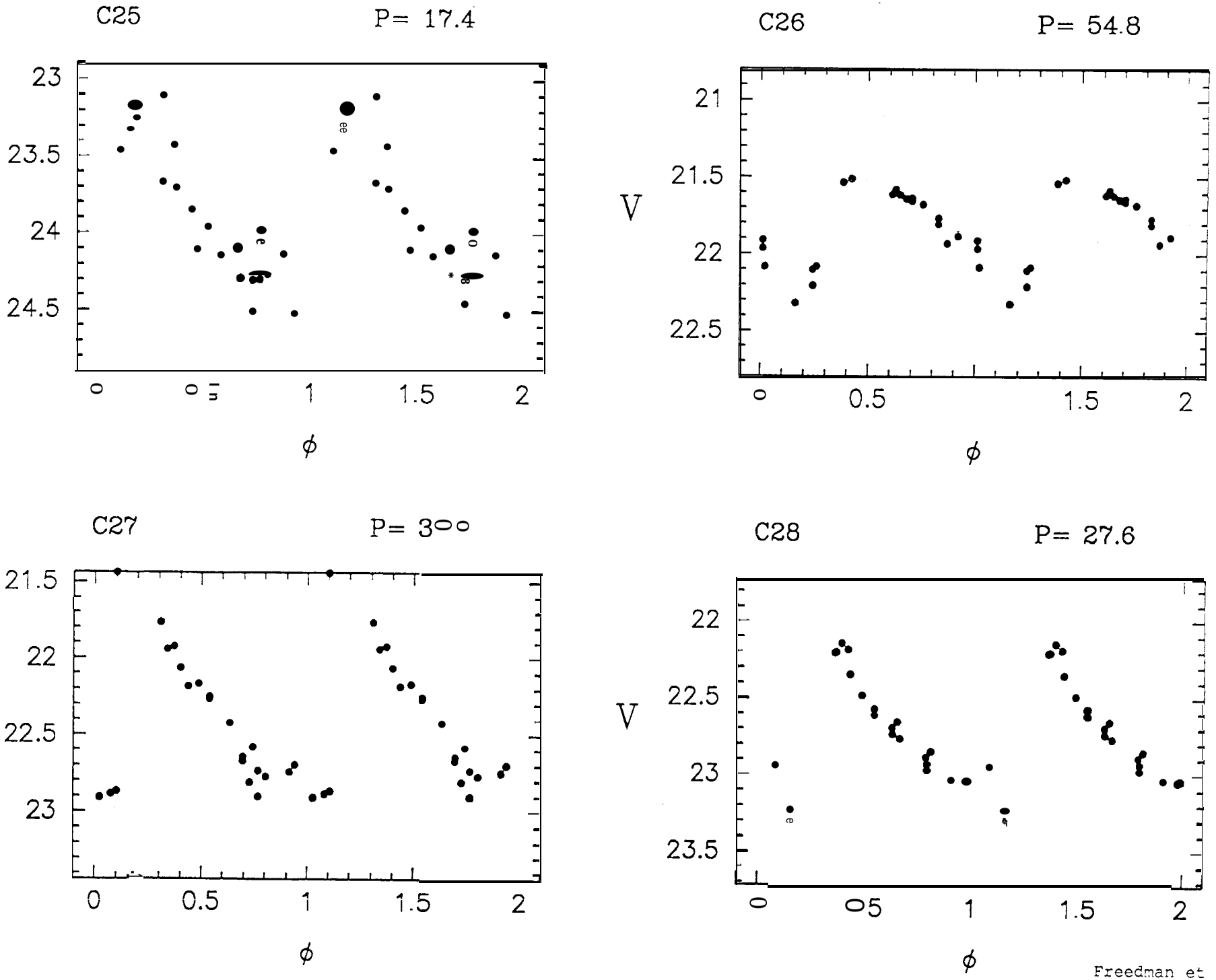

Freedman et al
Figure 8a

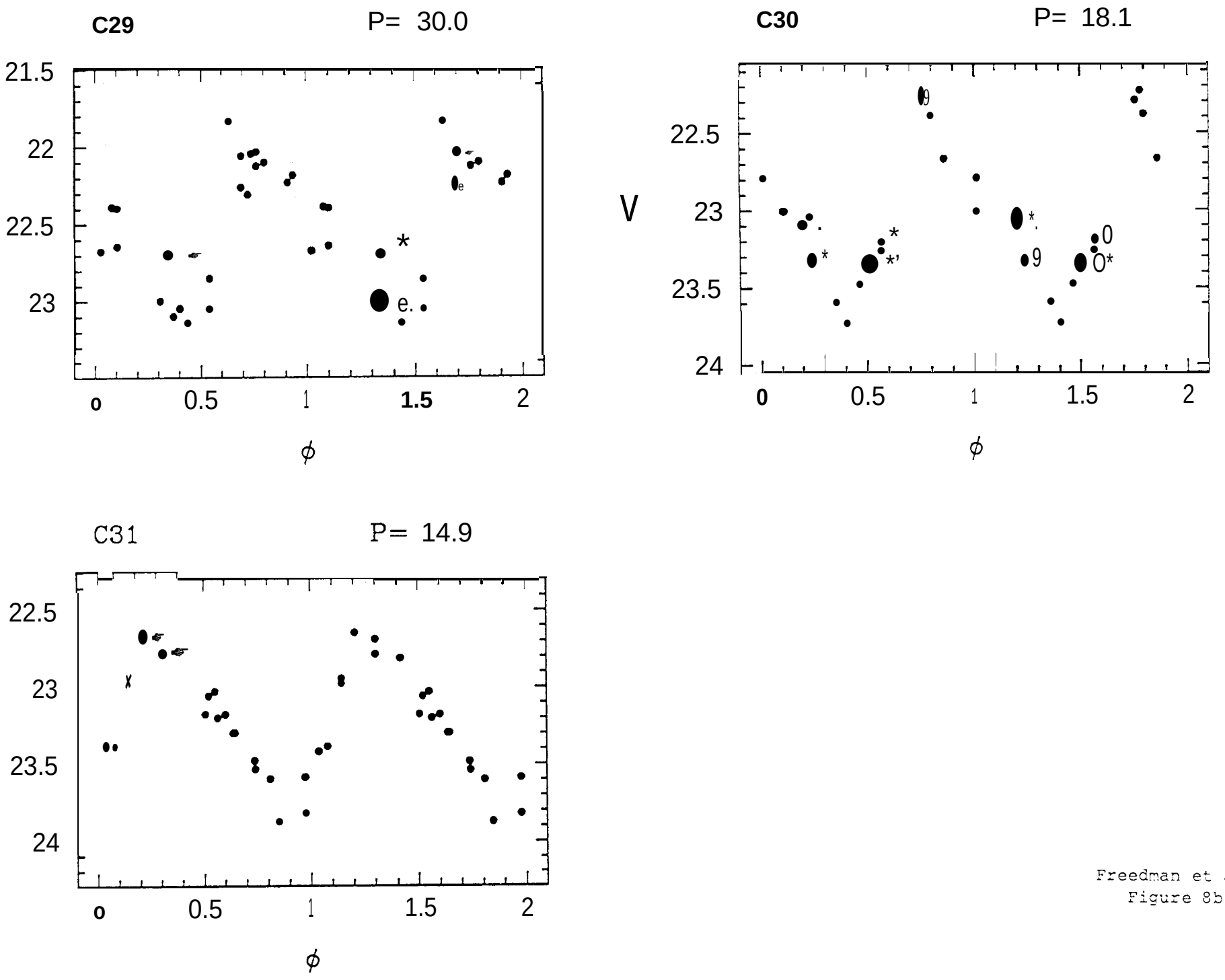

Freedman et al.
Figure 8b

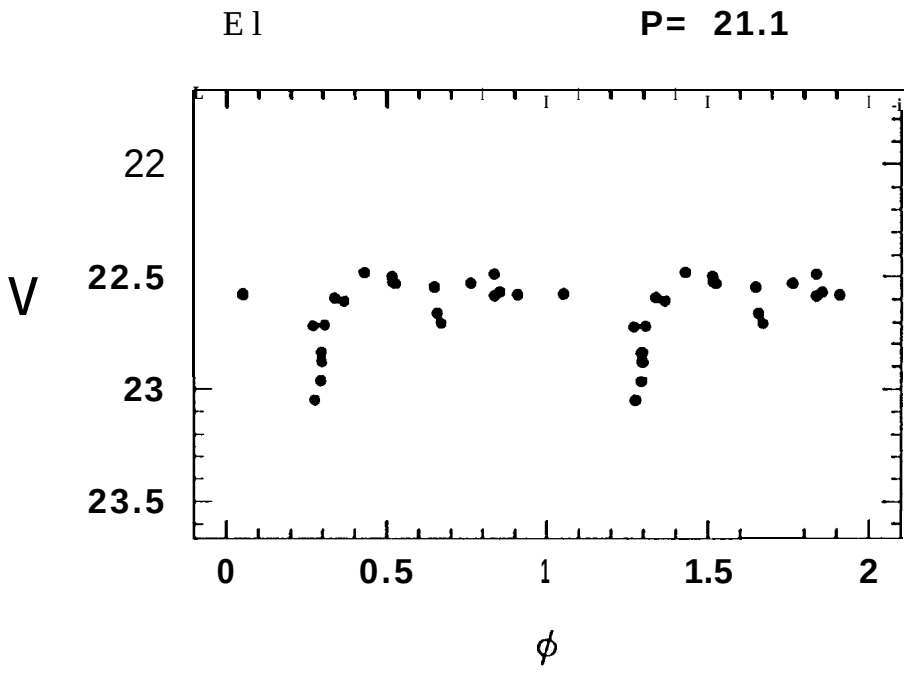

Freedman et al .
Figure 9

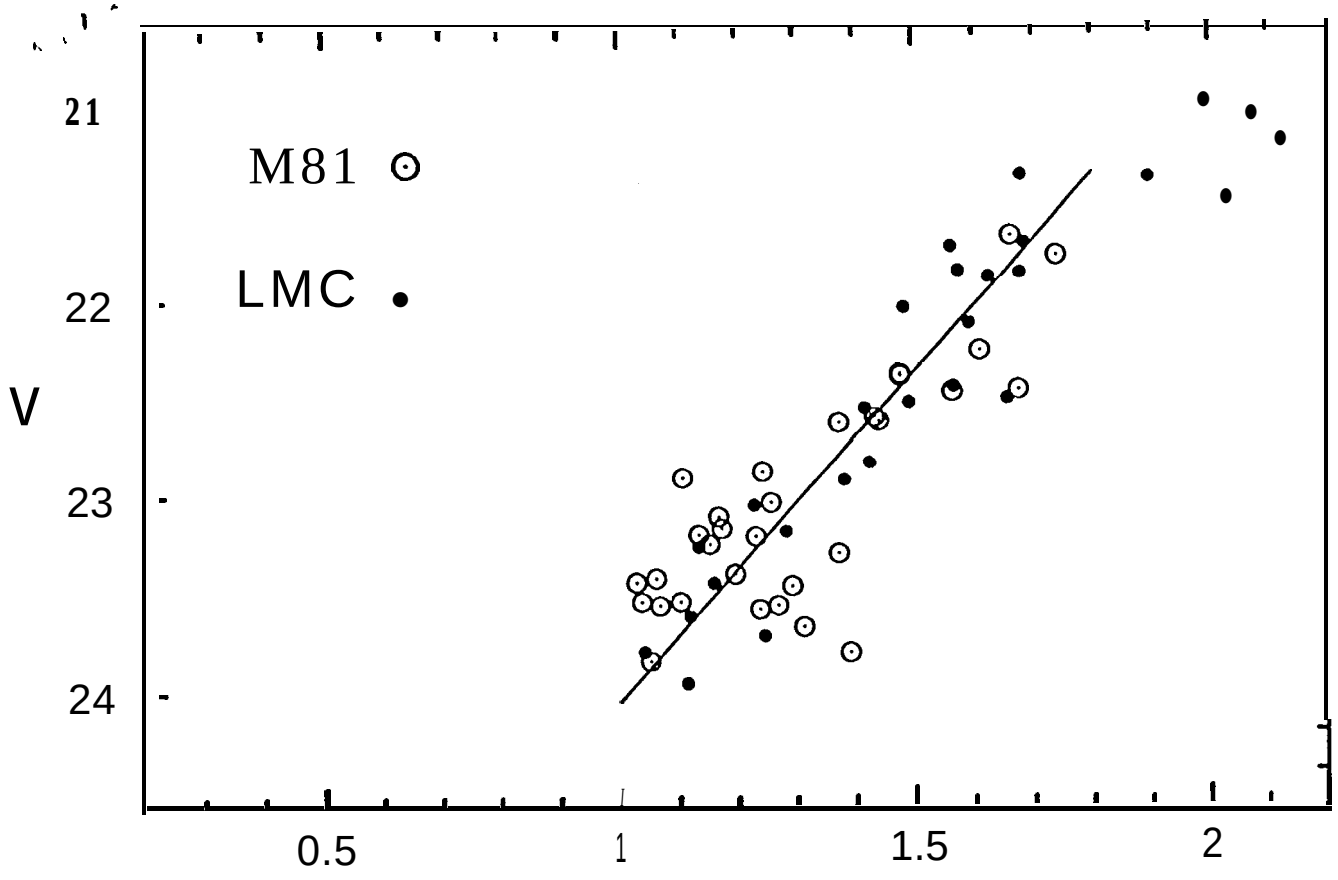

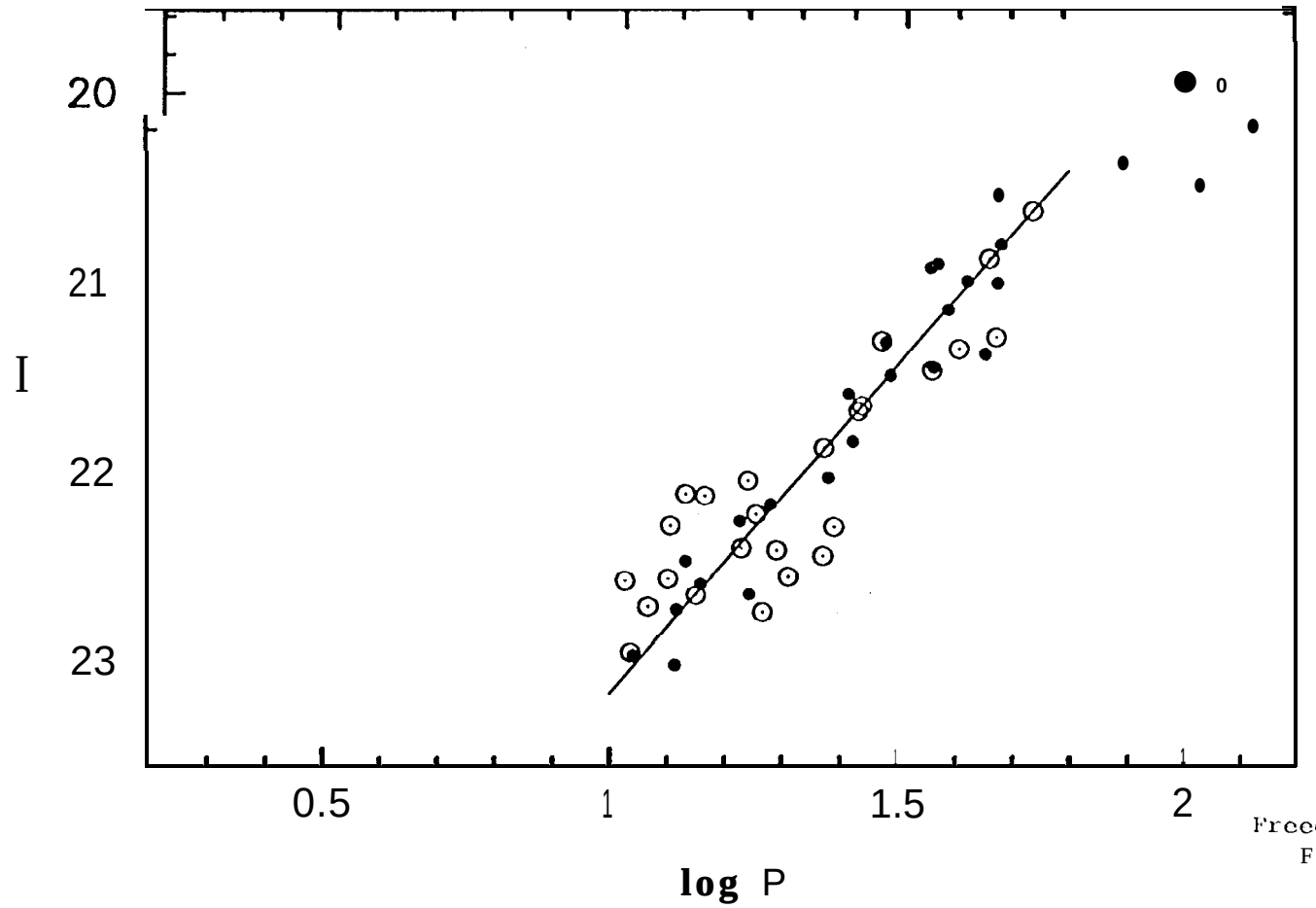

Freedman et al.
Figure 10

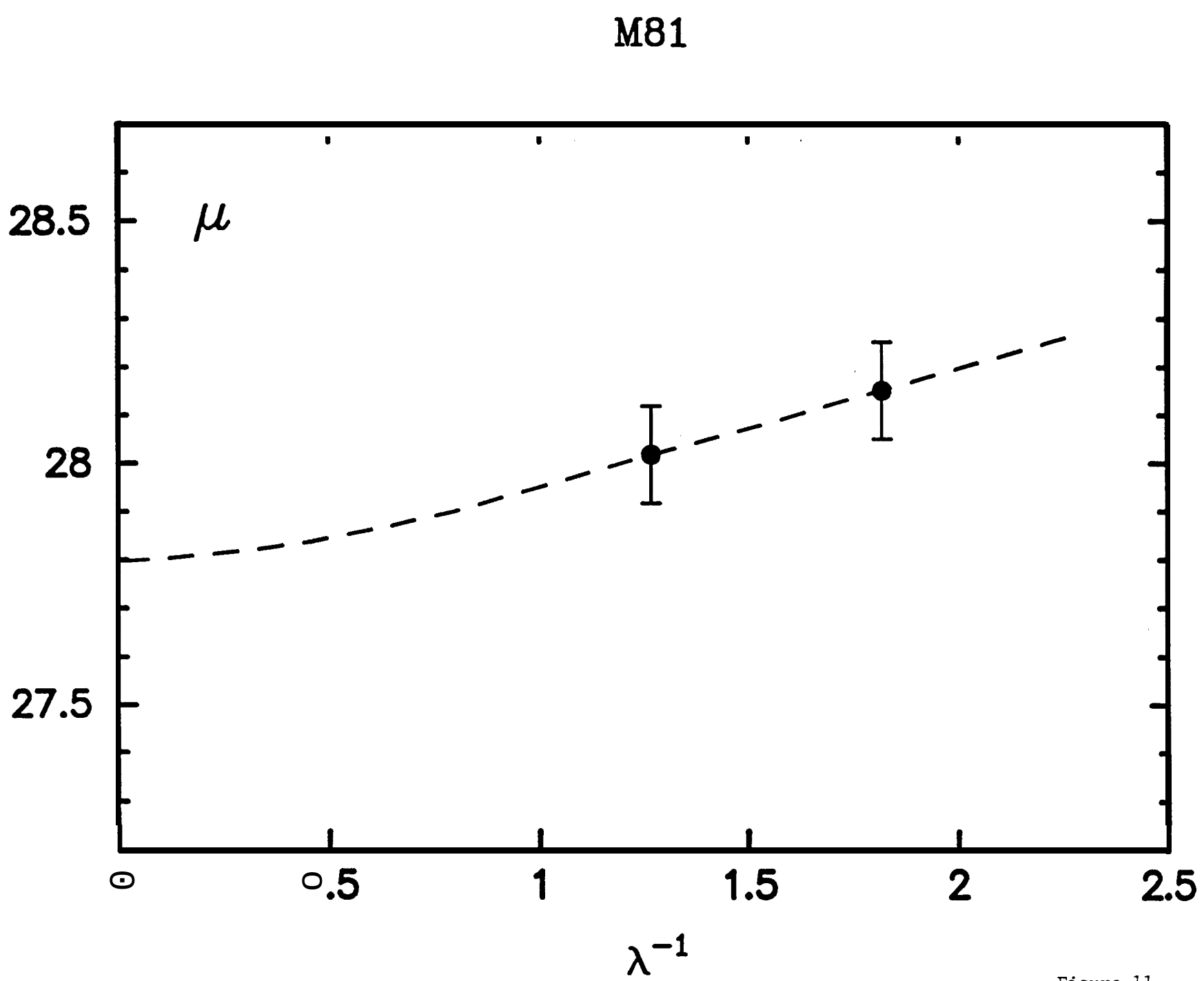

Figure 11